Bioactive Materials 9 (2022) 508–522

Contents lists available at ScienceDirect

Bioactive Materials

journal homepage: www.sciencedirect.com/journal/bioactive-materials

Rock inhibitor may compromise human induced pluripotent stem cells for cardiac differentiation in 3D

Bin Jiang [a], Wenquan Ou [a], James G. Shamul [a], Hao Chen [a], Sarah Van Belleghem [a], Samantha Stewart [a], Zhenguo Liu [b], John P. Fisher [a], Xiaoming He [a,c,*]

[a] Fischell Department of Bioengineering, University of Maryland, College Park, MD, 20742, United States
[b] Division of Cardiovascular Medicine, University of Missouri School of Medicine, Columbia, MO, 65212, United States
[c] Marlene and Stewart Greenebaum Comprehensive Cancer Center, University of Maryland, Baltimore, MD, 21201, United States

ARTICLE INFO

Keywords:
Episomal
iPSC
Cardiomyocyte
Spheroid
GelMA

ABSTRACT

Cardiomyocytes differentiated from human induced pluripotent stem cells (iPSCs) are valuable for the understanding/treatment of the deadly heart diseases and their drug screening. However, the very much needed homogeneous 3D cardiac differentiation of human iPSCs is still challenging. Here, it is discovered surprisingly that Rock inhibitor (RI), used ubiquitously to improve the survival/yield of human iPSCs, induces early gastrulation-like change to human iPSCs in 3D culture and may cause their heterogeneous differentiation into all the three germ layers (i.e., ectoderm, mesoderm, and endoderm) at the commonly used concentration (10 μM). This greatly compromises the capacity of human iPSCs for homogeneous 3D cardiac differentiation. By reducing the RI to 1 μM for 3D culture, the human iPSCs retain high pluripotency/quality in inner cell mass-like solid 3D spheroids. Consequently, the beating efficiency of 3D cardiac differentiation can be improved to more than 95 % in ~7 days (compared to less than ~50 % in 14 days for the 10 μM RI condition). Furthermore, the outset beating time (OBT) of all resultant cardiac spheroids (CSs) is synchronized within only 1 day and they form a synchronously beating 3D construct after 5-day culture in gelatin methacrylol (GelMA) hydrogel, showing high homogeneity (in terms of the OBT) in functional maturity of the CSs. Moreover, the resultant cardiomyocytes are of high quality with key functional ultrastructures and highly responsive to cardiac drugs. These discoveries may greatly facilitate the utilization of human iPSCs for understanding and treating heart diseases.

1. Introduction

Heart diseases are the leading cause of death in the United States [1,2]. A major reason for this is that the human heart has very limited capacity to regenerate cardiomyocytes (CMs) once they are damaged by some malfunction (e.g., ischemia), leading to myocardial infarction [3,4]. Stem cell therapy has been considered as a promising strategy for treating heart diseases [5–8]. It is well accepted now that functional/beating human CMs can be differentiated only from human pluripotent stem cells (PSCs) including human embryonic stem cells (ESCs) and induced pluripotent stem cells (iPSCs), although mesenchymal stem cells (including "cardiac stem cells") may be used for cardiac regeneration via their cytokine effect and differentiation into some cardiac stromal cells [3,4]. However, the human ESCs isolated from the inner cell mass of human embryos are associated with significant ethical concerns [9]. In contrast, human iPSCs reprogrammed from somatic cells (e.g., fibroblasts in the skin) are capable of differentiating into CMs with no ethical concerns [10,11]. Moreover, human iPSC-derived CMs can be used as not only a therapeutic agent for treating heart diseases, but also a valuable tool for elucidating the etiology and pathogenesis of heart diseases and developing engineered heart tissues to test the cardiotoxicity of pharmaceutical drugs [12–15].

To derive human CMs from iPSCs, contemporary efforts have been focused on using the cells attached on a 2D culture surface [16–18]. This procedure may be greatly limited by the area of culture surface for large-scale cell production. Besides, the 2D approach requires detaching or dissociating CMs from the surface/substrate, which may cause cell death and loss [19,20]. Notably, therapeutic applications typically require up to 10^8 -10^9 CMs per case, which can be practically achieved only by 3D culture with a scaled-up cell production [21,22]. Moreover,

Peer review under responsibility of KeAi Communications Co., Ltd.
* Corresponding author. Fischell Department of Bioengineering, University of Maryland, College Park, MD 20742, United States.
E-mail address: shawnhe@umd.edu (X. He).

https://doi.org/10.1016/j.bioactmat.2021.07.013
Received 11 April 2021; Received in revised form 15 July 2021; Accepted 15 July 2021
Available online 2 August 2021

3D culture better recapitulates the "niche" *in vivo* and may support the growth of PSCs with increased proliferation and pluripotency [23–25].

There are also a few studies reported on the differentiation of cardiac spheroids (CSs) containing CMs from human and non-human PSC (mostly ESCs) spheroids in 3D [24,26,27]. These 3D PSC-derived CSs can be used directly for tissue engineering and regenerative medicine without the need for dissociating/detaching them from a culture substrate. However, these protocols are lengthy (typically requiring at least 14 days) and generate CSs with high heterogeneity [28–30]. The latter is evidently reflected by the large variation of the outset beating time (OBT) of the CSs, which is typically over ~7 or more days for all contemporary 3D cardiac differentiation approaches [21,31]. The OBT is a direct indicator of the maturity of the PSC-derived CSs because their beating is a result of the maturation of the intra- and inter-cellular protein system that drives the motion. Hence, there is an urgent need to address the aforementioned concerns (i.e., heterogeneity and lengthiness) on current 3D cardiac differentiation protocols, by identifying the pivotal factor that leads to the high heterogeneity for optimizing the differentiation protocol to produce a sufficiently high number of quality iPSC-derived CMs in 3D for basic research, tissue engineering, and therapeutic applications in the clinic [14,15,32,33].

In this study, we discovered that Rock inhibitor (RI) that has been ubiquitously used as a medium supplement to prevent apoptosis during handling and culture of human PSCs including both human ESCs and iPSCs [21,23,34–37], compromises the capacity of cardiac differentiation of human iPSCs in 3D. Hence, we hypothesize that the RI concentration may be adjusted to achieve homogeneous cardiac differentiation of human iPSC in 3D. Indeed, by reducing the RI concentration for handling/culturing human iPSCs to derive CMs in 3D, we can improve cardiac differentiation with an OBT synchronized within 24 h (versus 7 or more days for all contemporary protocols) and shorten the time required for cardiac differentiation by at least 7 days. Furthermore, the resultant CSs from our protocol have up-regulated cardiac genes and proteins for maturation. In addition, iPSCs induced with episomal plasmids (eiPSCs) used in this study are virus-free, which minimizes the concern on their safety for clinical translation [38]. Eventually, this optimized protocol for cardiac differentiation of eiPSCs in 3D may be valuable for large-scale production of high-quality human CSs/CMs, to accelerate not only drug screening but also the understanding and treatment of the deadly heart diseases.

2. Results

2.1. Unprecedented capacity of 3D cardiac differentiation of human eiPSCs cultured in 3D with low RI

The timeline for the 4-day (from day −4 to 0) 3D culture and the subsequent 3D cardiac differentiation of iPSCs in this study is illustrated in Fig. 1a. First, 3D eiPSC spheroids are obtained for 3D cardiac differentiation, for which the eiPSC colonies from 2D culture are detached and mechanically cut with a cell strainer (100 μm mesh size) into small iPSC clumps for suspension culture in the mTeSR medium for 4 days. Methylcellulose is added into the medium to enhance the medium viscosity and reduce fusion of the eiPSC clumps/spheroids during the suspension culture [26]. During the first two days of 3D culture, the medium was supplemented with 1 μM RI (low RI), 5 μM RI, or 10 μM RI (high RI that has been commonly used for improving the survival/yield of human PSCs including iPSCs during culture) [23,34], and no RI is used during the last two days of culture. Typical images showing the morphology of the iPSC spheroids under suspension culture on days −3 and 0 from both the 1 and 10 μM RI groups are given in Figs. S1a–b. The size (in diameter) distributions of the eiPSC spheroids on day 0 for both groups are given in Fig. S1c: The spheroids are 245.3 ± 42.0 μm and 227.9 ± 38.5 μm and there are 3172 ± 272 and 2662 ± 207 cells per spheroid, for the 1 and 10 μM RI groups, respectively. The pluripotent nature of the eiPSC spheroids from both groups are confirmed by their capability of forming teratomas consisting of tissues from all the three germ layers (i.e., neural epithelium, cartilage, and gut epithelium for ectoderm, mesoderm, and endoderm, respectively, Fig. S2).

Cardiac differentiation of the 3D eiPSC spheroids is conducted by modulating the canonical Wnt signaling pathway with agonists and antagonists sequentially, which has also been used for differentiation of human PSCs into CMs under 2D culture [16,18]. Two Wnt agonists, CHIR99021 (8 μM) and 6-bromoindirubin-3′-oxime (BIO, 2 μM), are supplemented into the culture medium on day 0, to up-regulate the Wnt signaling and induce iPSC differentiation into mesoderm for 1 day. On day 1, two Wnt antagonists, XAV939 (10 μM) and KY02111 (10 μM), are used to suppress the Wnt signaling for inducing cardiac commitment of the mesoderm cells in the following 6 days to obtain beating CSs. Afterward, the CSs are cultured in pure cardiac maintenance medium for maturation till day 13.5. Spontaneous beating can be observed for ~48 % of the CSs in the 1 μM RI group on as early as day 6.5, and the percentage of beating CSs is peaked at ~97 % at ~24 h later on day 7.5 (Fig. 1b and Movie 1). In other words, the outset beating time (OBT) of the CSs is synchronized to be within ~24 h for the 1 μM RI group. No significant change in the beating percentage from day 7.5 to day 13.5. In contrast, in the 10 μM RI group, only ~8 % and ~44 % of CSs beat on days 6.5 and 13.5, respectively (Fig. 1b and Movie 2, on day 13.5). Moreover, the 5 μM RI group shows a shortened OBT of 3 days (from day 6.5 to day 9.5) and ~61 % beating CSs on days 9.5 (Fig. 1b). Therefore, the OBT ranges over at least a week, indicating high heterogeneity of the CSs in the 10 μM RI group as the beating is a direct and visible indicator of functional maturity of the CSs. In other words, the 3D cardiac differentiation of eiPSCs in the 5 and 10 μM group is not only significantly less efficient (and lengthier) but also less homogeneous than that in the 1 μM RI group.

Supplementary video related to this article can be found at https://doi.org/10.1016/j.bioactmat.2021.07.013.

To further investigate the difference of cells in CSs between the 1 and 10 μM RI groups, the CSs on day 13.5 from both groups are re-plated in regular cell culture petri dish. After 3 days, ~61 % of the CSs in the 10 μM RI group attach to the 2D surface, and some of the cells migrated out of the spheroids appear to be neuron-like with neurite-like processes (Fig. 1c–d and Movie 3). In contrast, less than 5 % of the CSs in the 1 μM RI group become attached after the re-plating and migration of cells out of the CSs is negligible, while the 5 μM RI group shows ~41 % attached CSs (Fig. 1c–d and Movie 4). Moreover, both the percentage of cTnT-positive cells in the CSs and the mean intensity of cTnT fluorescence staining (representing the cTnT protein expression in the CSs) decreases with the increase of the RI concentration from 1 to 10 μM RI (Fig. S3), showing high concentration of RI compromises the cardiac differentiation of the human eiPSCs. To confirm the aforementioned observation of neuron-like cells in the 10 μM RI group, immunofluorescence staining of cryosectioned CSs on day 12.5 in the 1 and 10 μM RI groups is conducted. Indeed, cells that are positive for neural lineage markers TUJ-1 and MUSASHI can be observed in the CSs from the 10 μM RI group (Fig. 1e). In stark contrast, no evident staining of MUSASHI and TUJ-1 is observable in the CSs from the 1 μM RI group. Furthermore, the cardiac sarcomere-specific protein cTnT and gap junction (for conduction of cardiac potential) protein CONNEXIN-43 (CX-43) are highly expressed in the CSs of the 1 μM RI group (Fig. 1f), while their expression is either weak (for cTnT) or barely visible (for CX-43) in the CSs of the 10 μM RI group. Taken together, these data show that the 10 μM RI compromises cardiac differentiation of eiPSCs in 3D with a noticeable existence of neuron-like cells, and by reducing the RI to 1 μM, a protocol is developed to achieve highly efficient and synchronized cardiac differentiation of the eiPSCs in 3D. Therefore, studies are performed to further understand the mechanisms of the improved cardiac differentiation with the reduced RI.

Supplementary video related to this article can be found at https://doi.org/10.1016/j.bioactmat.2021.07.013.

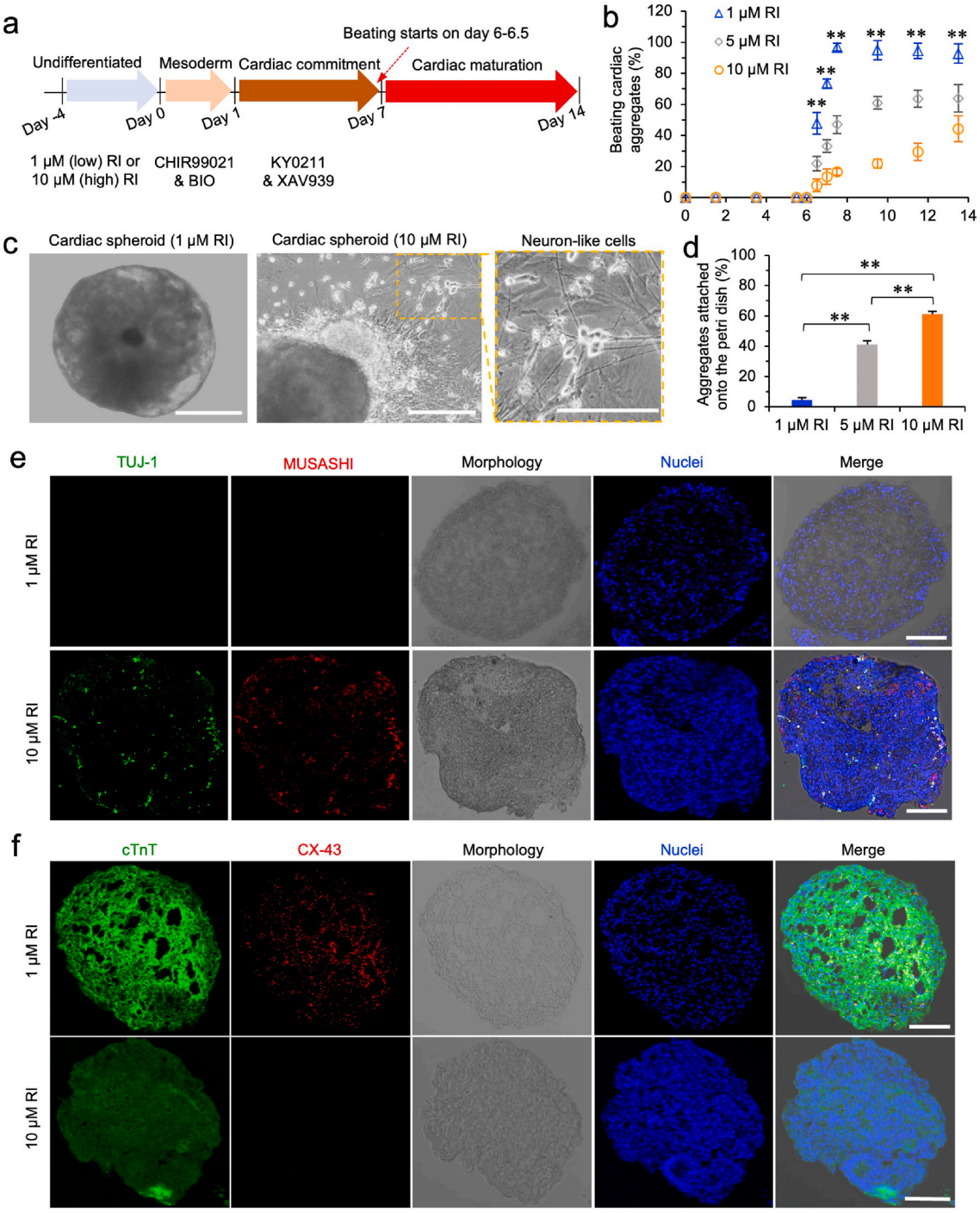

Fig. 1. Characterization of cardiac spheroids differentiated from eiPSCs made with 1, 5, and 10 μM RI in the medium before cardiac differentiation. (**a**) A schematic illustration of the timing for making the 3D eiPSC spheroids in 4 days and subsequently differentiating the eiPSCs into 3D cardiac spheroids (CSs). Either 1, 5, or 10 μM Rock inhibitor (RI) is supplemented into the eiPSC medium for culturing the 2D eiPSCs into eiPSC spheroids under 3D suspension culture. The eiPSC spheroids on day 0 are cultured with CHIR99021 and BIO in a mesoderm induction medium for 1 day to induce mesoderm differentiation. Afterward, KY02111 and XAV939 are supplemented in the cardiac maintenance medium to culture the spheroids for 6 days for cardiac commitment to obtain the CSs. Lastly, cardiac maintenance medium without KY02111 and XAV939 is used to culture the CSs for cardiac maturation. The CSs are observed to start to beat on days 6–6.5. (**b**) Quantitative data showing the percentage of beating CSs over time during a period of 13.5 days post the initiation of cardiac differentiation on day 0. Approximately 97 % of the CSs in the 1 μM RI group start to beat within 24 h, while 44.3 % of CSs are observed to beat over more than 7 days (from day 6–6.5 to day 13.5) for the 10 μM RI group, and 61 % of CSs are observed to beat over more than 3 days (from day 6–6.5 to day 9.5) for the 5 μM RI group. (**c**) The morphology of CSs (obtained on day 13.5 of cardiac differentiation) was transferred into a regular cell culture petri dish and cultured for 3 days. The CSs in the 1 μM RI group maintain the spheroidal shape with few cells attached to the surface. Many cells in the CSs in the 10 μM RI group migrate out and attach to the petri dish with fibroblast-like and neuronal-like morphology. (**d**) Quantitative data showing few CSs in the 1 μM RI group attach on the surface while >60 % CSs in the 10 μM RI group and 41 % CSs in the 5 μM RI group attach on the surface. (**e**) Immunostaining data showing there are cells positive for the neural-specific markers (TUJ-1 and MUSASHI) in the CSs of the 10 μM RI group, while it is not observable for the CSs of the 1 μM RI group. (**f**) Immunostaining data showing much higher expression of the cardiac-specific protein markers (cTnT and CX-43) in the CSs (collected on day 12.5) of the 1 μM RI group than the 10 μM RI group. Scale bars: 100 μm **, $p < 0.01$.

Table 1
Sample groups and their abbreviations for RNA-sequencing studies.

RI dosage	Undifferentiated (U)	Cardiac commitment (C)	Cardiac maturation (M)	2D control (2D)
1 μM (One, O)	UO	CO	MO	2D
10 μM (Ten, T)	UT	CT	MT	

2.2. High RI-induced heterogeneous gene expression of eiPSCs under 3D culture to compromise their 3D cardiac differentiation

To investigate the mechanisms for the different outcomes when using different RI concentrations for culturing the eiPSC spheroids in 3D for cardiac differentiation, samples at various stages of the 3D culture and differentiation shown in Fig. 1a are collected and analyzed by RNA-sequencing (RNA-seq). The sample groups are summarized in Table 1 including undifferentiated eiPSCs on day −2.5 (U), cardiac commitment on day 2.5 (C), cardiac maturation on day 13.5 (M), together with 2D monolayer colonies on day −4 (2D) as a common 2D undifferentiated control for both the 1 (one: O) and 10 (ten: T) μM RI 3D culture. The raw data of RAN-seq are of high quality with an error rate of no more than 0.03 % (Table S1). The raw data passed quality control are then aligned for mapping to the reference (human genome) [39] with a total mapping rate of 95.8 ± 0.5%. Afterward, the gene expression level is calculated by the number of mapped reads, also known as fragments per kilobase of transcript per million mapped reads (FPKM) [40]. Moreover, the global transcriptome of different samples with cluster analysis and hierarchical clustering analysis is carried out with $\log_{10}$(FPKM+1) on differentially expressed genes within all comparison groups and plotted as a heat-map (Fig. S4), showing the global gene expression pattern of samples together with the samples' hierarchies that match with the different stages of the different samples given in Fig. 1a.

To understand the number of genes that are uniquely expressed in each group (i.e., 1 μM RI, 10 μM RI, or 2D) and co-expressed in two or all of the three groups at different stages of 3D culture and cardiac differentiation as compared to the 2D control, the Venn diagrams are generated and shown in Fig. S5. The total number of co-expressed genes are similar in three groups at all three stages (UO/UT/2D: 12450, CO/CT/2D: 12505, and MO/MT/2D: 11848), but the differentially expressed unique genes increased from undifferentiated stage to cardiac commitment and then cardiac maturation (UO/UT/2D: 123/173/451, CO/CT/2D: 359/103/464, and MO/MT/2D: 549/521/907). This is further shown in the Volcano plots of the overall distribution of differentially expressed genes with a threshold being less than 0.05 for the adjusted *p* value (padj) [41] (Fig. S6). This trend of increased significantly differentially expressed genes with the advance of the stage of differentiation is due to the increased expression of somatic genes from the early to late stages of cardiac differentiation.

The differentially expressed genes are further examined through an enrichment analysis with the Gene Ontology (GO) database as reference [42], to determine the biological functions or pathways significantly enriched with the genes. Notably, the top 18 significantly upregulated differentially expressed gene groups of MO with regard to MT (MO vs. MT) are enriched to heart development, muscle system process, and the development of Z-disc and I band (Fig. 2a), suggesting that the CMs in the MO group have improved development/maturation in sarcomere organization compared to the CMs in the MT group. The top 2 significantly down-regulated differentially expressed gene groups of MO vs. MT are enriched to the forebrain and axon development of the ectoderm-derived lineages (Fig. 2b). As expected, the CMs in both MO and MT groups show a prominent upregulation of differentially expressed gene groups enriched to heart development compared to the control 2D group (MT vs. 2D: top 2 in Fig. 2c and MO vs. 2D: top 1 in Fig. 2d). Notably, MT has many differentially expressed genes enriched to heterogeneous endoderm (e.g., embryonic development of organs like lung and gut) and non-cardiac mesoderm (e.g., cartilage and urogenital) tissue development, in addition to the ectoderm tissue (e.g., eye) development (Fig. 2c,e), which is not observed for MO (Fig. 2d). The enriched functional clusters with detailed genes are plotted in a heat-map in addition to the expression of pluripotent genes (e.g., *POU5F1*, *SOX2*, *NANOG*, and *DNMT3B*) that are all decreased in MO and MT (Fig. 2e and Fig. S7). Importantly, SOX2 which is important for neural stem cell development has higher expression in MT than MO, which indicates an increased shift toward the neural lineage of cells in the MT group compared to the MO group. Interestingly, the early cardiac-associated genes (e.g., *SALL4*, *NTN1*, and *GLI1*) are expressed as early as the undifferentiated stage (U) when the pluripotency genes are dominant in the transcriptome (Fig. 2f and Fig. S7, S8a-b). There are upregulated genes enriched to heart development in UO compared to UT (Fig. S8c). Furthermore, genes (e.g., *FGF8*, *ID1*, *NODAL*, *SKOR2*, and *LEFTY2*) enriched to the BMP signal pathway involving in cardiogenesis [43], are upregulated in UO compared to UT (Fig. 2f and Fig. S8c). In addition, upregulated genes enriched to cell adhesion are also present in UO compared to UT (Fig. S8c). However, the genes enriched to RNA transcription and metabolism are down-regulated in UO but up-regulated in UT compared to 2D (Fig. 2f and Fig. S8d). Moreover, there are neural tube closure associated genes (e.g., *COBL*, *ST14*, *SEMA4C*, and *SETD2*) [44,45] upregulated in UO compared to UT, while pro-neural development genes (e.g., *DACT1*, *SFRP2*, *FOXB1*, and *HES3*) [46,47] are upregulated in UT compared to UO (Fig. 2f). At the intermediate CO/CT stage, it shows significantly upregulated expression of genes (e.g., *LGR4*, *LRP2*, *GATA3*, *BMP5*, *HAND1*, *MSX2*, and *PDGFRA*) enriched to heart development in the CO group compared to the CT group (Fig. 2f and Fig. S9).

2.3. High RI-induced heterogeneous protein expression of eiPSCs under 3D culture to compromise their 3D cardiac differentiation

The heterogeneous protein expression induced by high RI is first indicated by the morphology of the eiPSC spheroids (Figs. S1a–b): nearly all the eiPSC spheroids after one-day culture on day −3 in the 10 μM RI group have an archenteron-like cavity (although it becomes less evident on day 0, probably due to the inward growth of the cells into the cavity). This is not observable for the iPSC spheroids that remain solid-like in the 1 μM RI group, similar to the solid-like inner cell mass that contains pluripotent (i.e., embryonic) stem cells in the early stage of blastula (Fig. S10a). This structure of cell aggregates with an archenteron-like cavity (Figs. S1a–b) for the 10 μM RI group resembles that of the epiblast and hypoblast-like cells (differentiated from the solid inner cell mass after invagination during early gastrulation, Fig. S10b) [48,49]. The aforementioned morphological difference of the eiPSC spheroids treated with 1 μM RI and 10 μM RI on day −3 is further confirmed with SEM imaging (Fig. S1b). Hence, we examined the expression of pluripotency and ectoderm differentiation protein markers within the eiPSC spheroids after four-day culture from the 1 and 10 μM RI groups using flow cytometry. As shown in Fig. 3a-b, the expression of three pluripotency markers including OCT-4, NANOG, and SSEA-4 is significantly higher in the 1 μM RI group, judged by the median fluorescence intensity and percentage of positive cells for the pluripotency markers. Furthermore, the expression of the ectoderm maker NESTIN is high (73.1 %) in the 10 μM RI group. In stark contrast, the expression of NESTIN is negligible in the 1 μM RI group. This is further confirmed by immunostaining of cryo-sectioned slices of the eiPSC spheroids with the various pluripotency and ectoderm markers (Fig. 3c-d). This unexpected

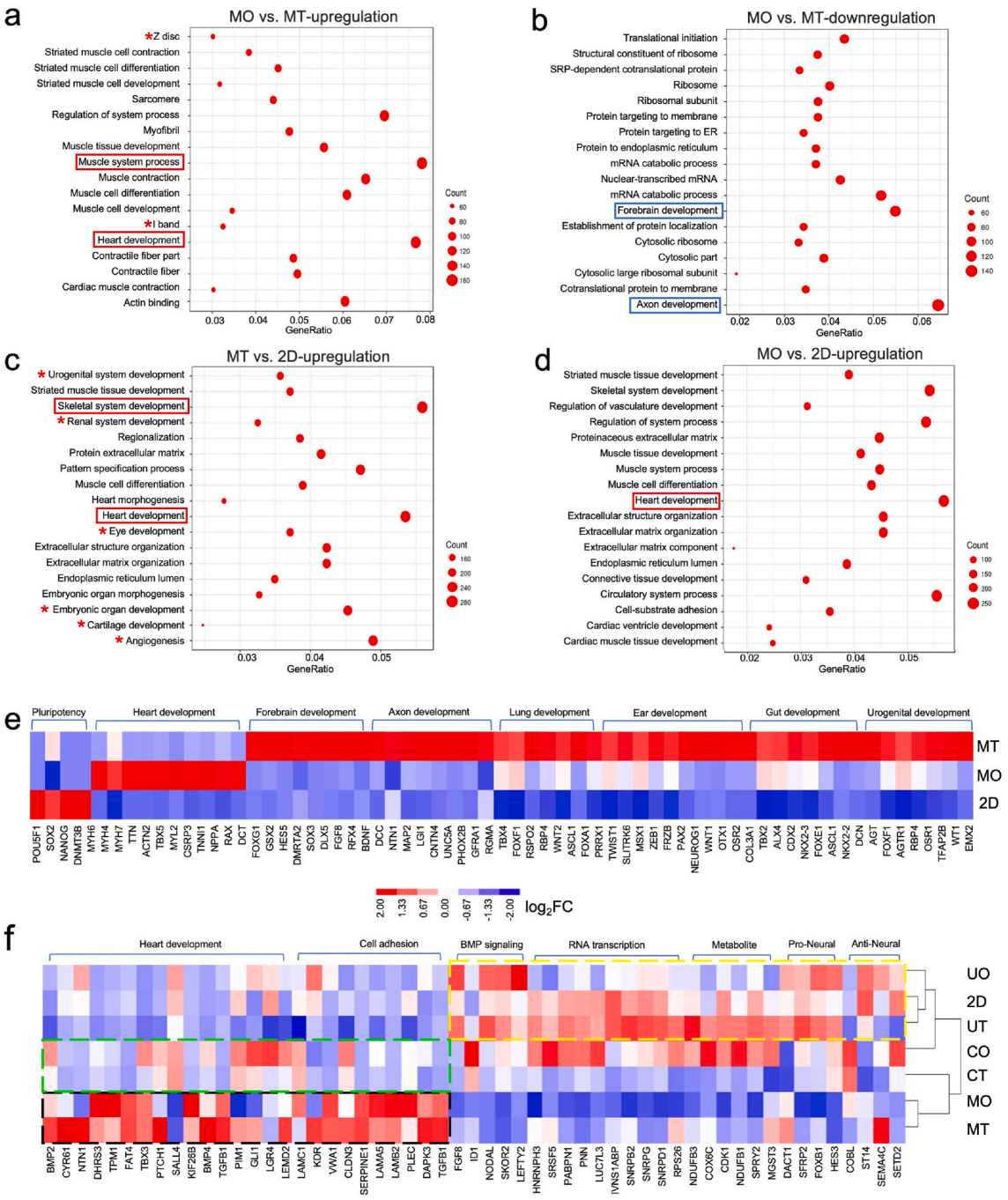

Fig. 2. Transcriptomic analysis of cardiac differentiation of eiPSCs cultured with 1 vs. 10 μM RI in the medium before cardiac differentiation. The 3D undifferentiated (U), cardiac commitment (C), and cardiac maturation (M) stages for both the 1 (one, O) and 10 (ten, T) μM RI groups together with the 2D cultured eiPSCs are analyzed. (**a**) Gene Ontology (GO) enrichment histogram displaying the top 18 significantly upregulated differentially expressed gene groups for MO with respect to MT (MO vs. MT). The red square boxes indicate the top 2 groups of upregulated genes are enriched to heart development and muscle system process. (**b**) GO enrichment histogram displaying the top 18 significantly downregulated differentially expressed gene groups for MO vs. MT. The blue square boxes indicate the top 2 groups of downregulated genes are enriched to forebrain development and axon development. (**c**) GO enrichment histogram displaying the top 18 significantly upregulated differentially expressed gene groups for MT vs. 2D. The red square boxes indicate the top 2 groups of upregulated genes are enriched to skeletal system development and heart development. Others are enriched to heterogeneous tissue development including the urogenital/renal system development, eye, cartilage, and angiogenesis, as indicated by asterisks. (**d**) GO enrichment histogram displaying the top 18 significantly upregulated differentially expressed gene groups for MO vs. 2D. The red box indicates the top upregulated gene group is enriched to heart development. (**e**) Heat-map displaying the transcriptional differences between the MT, MO, and 2D groups. The pluripotency genes are downregulated in both MT and MO; and heart development genes associated with sarcomere maturation and ion channels are upregulated in MO compared to MT, while more genes associated with heterogeneous tissue development including forebrain, axon, lung, ear, gut, kidney are upregulated in MT. (**f**) Heat-map displaying the transcriptional differences among the UO, 2D, UT, CO, CT, MO, and MT groups. The genes associated with the BMP signaling pathway are upregulated in UO compared to UT, while the RNA transcription and metabolism genes are downregulated in UO and upregulated in UT (indicated in the dashed yellow box). Subsequently, genes enriched to heart development of cardiac commitment show more early up-regulation in CO than CT (indicted in the dashed green box), which carries further into the cardiac maturation stage (MO vs. MT, in the dashed black box). The adjusted *p* value (padj) is less than 0.05 for all the genes given in **a**-**d** where the count indicates the number of enriched genes. $\log_2$FC: $\log_2$ (fold difference). The positive and negative numbers in **e**-**f** represent up- and downregulation, respectively.

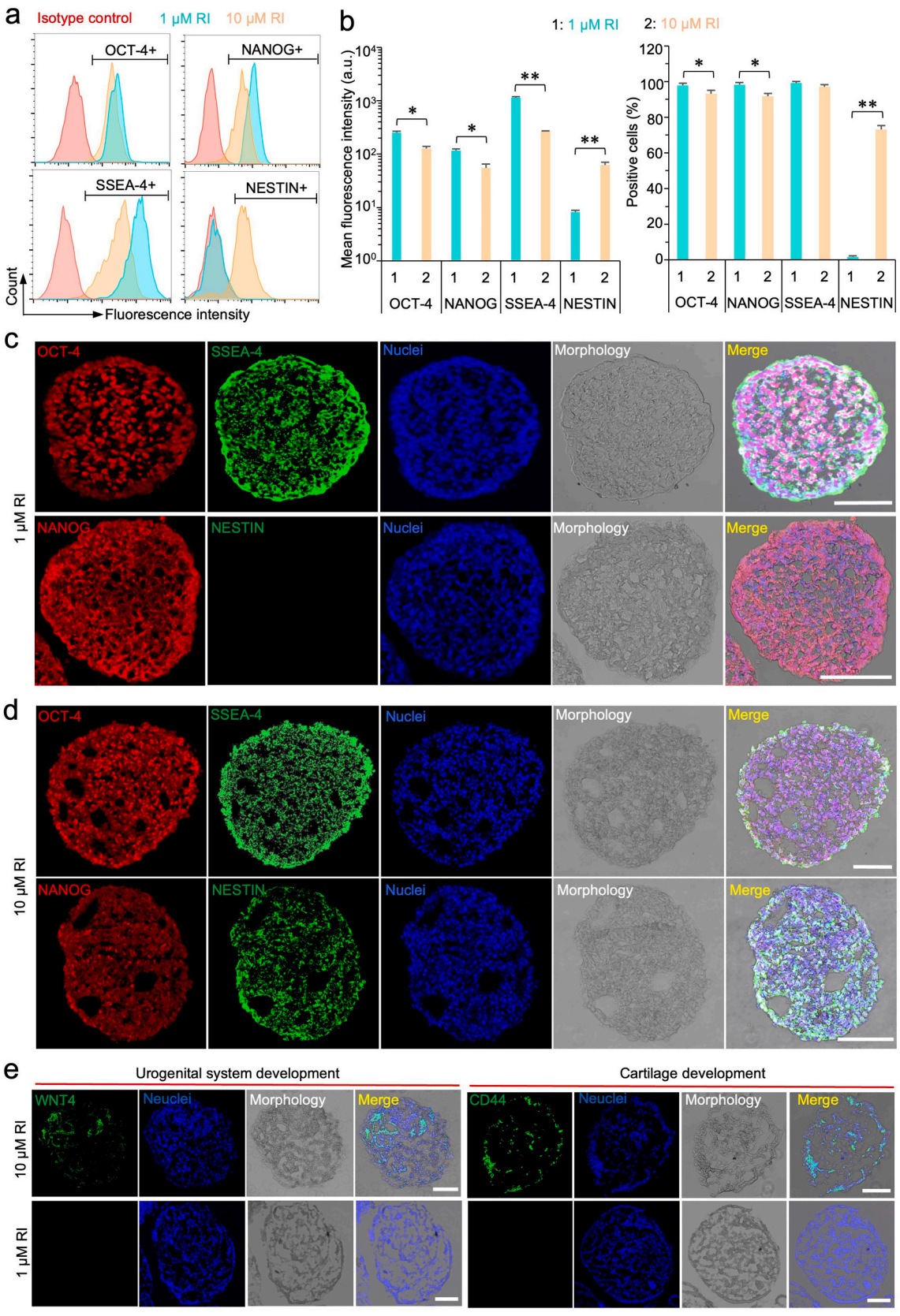

(caption on next page)

Fig. 3. Characterization of the eiPSCs under 3D suspension culture with 1 vs. 10 μM RI. (**a**) Representative peaks from flow cytometry analyses showing higher expression of the pluripotency protein markers OCT-4, NANOG, and SSEA-4 and lower expression of the ectoderm protein marker NESTIN in the eiPSCs (collected on day 0) from the 1 μM RI group than 10 μM RI group. (**b**) Quantitative data from the flow cytometry analyses showing cells in the 1 μM RI group have a significantly higher expression (represented by the mean fluorescence intensity) of all the three pluripotency markers and lower expression of the ectoderm maker than cells in the 10 μM RI group. Furthermore, significantly more cells are positive for two of the three pluripotency markers (OCT-4 and NANOG) and significantly fewer cells are positive for the ectoderm marker in the 1 μM RI group than the 10 μM RI group. (**c**) Immunostaining data showing high expression of all the three pluripotency markers (OCT-4, NANOG, and SSEA-4) and no evident expression of the ectoderm marker NESTIN in eiPSCs (collected on day 0) of the 1 μM RI group. (**d**) Immunostaining data showing evident expression of not only the three pluripotency markers but also the ectoderm marker in the eiPSCs (collected on day 0) of the 10 μM RI group. (**e**) Immunostaining data showing cells positive for the WNT4 and CD44 (which are markers for urogenital system and cartilage development, respectively) in the CSs of the 10 μM RI group, but not the 1 μM RI group. All the CSs are collected on Day 12.5 post-cardiac differentiation. Scale bars: 100 μm *, $p < 0.05$, and **, $p < 0.01$.

ectoderm induction of human iPSCs by the 10 μM RI under 3D culture may compromise their capability of differentiating into cells of non-ectoderm origin including CMs.

To further confirm the aforementioned difference in morphology and protein expression between the 1 and 10 μM RI groups, the 3D iPSC spheroids obtained with 0, 1, and 10 μM RI concentrations collected on day 0 (i.e., after 4-day culture in 3D) are plated on the 2D surface coated with Matrigel in Petri dish (i.e., under conventional 2D culture) and cultured for 2 days to observe the cell morphology. Although eiPSC colonies are observable for all the three groups, the ones in the 0 and 1 μM RI groups are typical with tightly packed cells consisting mainly of nuclei inside them and a largely smooth outer boundary (Fig. S11a). In contrast, the cells in the eiPSC colonies of the 10 μM RI group are more loosely packed with a reduced ratio (in volume) of nuclei to the cytoplasm and the colonies have a largely spiky outer boundary with sprawled-out differentiated cells (Fig. S11a), suggesting spontaneous differentiation of the eiPSCs in the 10 μM RI group during culture. This is confirmed by the immunostaining data of the iPSCs spheroids shown in Figs. S11b–c: positive staining of neural markers (NESTIN and TUJ-1) and weakened/no staining of pluripotency markers (OCT-4 and NANOG) are observable in the colonies of the 10 μM RI group; in contrast, the colonies of the 0 and 1 μM RI groups show positive expression of OCT-4 and NANOG and are negative for NESTIN and TUJ-1.

Lastly and importantly, protein markers for urogenital system development (WNT4) [50,51] and cartilage development (CD44) [52,53] are also observable in the eiPSC-derived CSs of the MT group but not the MO group (Fig. 3e), confirming at the protein expression level, the heterogeneous non-cardiac mesoderm tissue development in the MT (but not MO) group identified earlier by the RNA-seq gene analysis (Fig. 2c). Collectively, the commonly used high concentration (10 μM) RI causes heterogeneous differentiation of eiPSCs under 3D culture and adversely compromises their cardiac differentiation in 3D, which may be overcome by reducing the RI concentration to 1 μM. Therefore, the quality of cardiac differentiation of the eiPSC spheroids from the low (1 μM) RI group is further studied.

2.4. Characterization of high-quality cardiac differentiation of iPSCs in 3D with low RI

Probably due to the high and homogeneous pluripotency of the eiPSC spheroids in the low RI group according to the aforementioned transcriptomic and protein analyses, the cardiac differentiation procedure results in high purity of cells at each of the three stages of modulating the Wnt signal pathway (Fig. 4a-d). After incubation with agonists of Wnt signaling (CHIR99021 and BIO) for 1 day, the eiPSCs are successfully induced into the mesoderm lineage. This is confirmed by the highly and homogeneously positive staining for the mesoderm protein marker BRACHYURY in the spheroids (Fig. 4a) and the ~100 % BRACHYURY-positive cells in the spheroids according to flow cytometry analysis (Fig. 4d). Afterward, the mesoderm cells are induced with antagonists of Wnt signaling (XAV-939 and KY02111) for 1.5 days to commit to the cardiac lineage on day 2.5, which is confirmed with the homogeneous (Fig. 4b) and high (~100 %, Fig. 4d) expression of the cardiac progenitor cell protein marker NKX2.5. After further cardiac commitments to day 6 and cardiac maturation to day 12.5, the CSs have abundant sarcomeres with a homogeneous expression of myofibril-associated protein α-ACTININ and intermediate filament protein DESMIN, showing advanced development of sarcomere organization (Fig. 4c). This is further confirmed by quantitative analyses of the sarcomere-related proteins including α-ACTININ and cTnI, which shows more than 90 % of the cells in the CSs on day 12.5 are positive for the two protein markers (Fig. 4d). In contrast, cells positive for the neural lineage cell makers MUSASHI and TUJ-1 are negligible (Fig. 4d and Fig. S12), indicating a high-quality cardiac differentiation via the reduction of RI concentration for culturing the eiPSCs in 3D before initiating cardiac differentiation to minimize their heterogeneous differentiation.

The quality of the CSs in the low RI group on day 12.5 is further analyzed with transmission electron microscopy (TEM) to identify the key CM functional ultrastructures [14]. As shown in Fig. 5a, the CMs in the CSs developed plenty of myofibrils (MF, up to 18 μm) and sarcoplasmic reticula (SR), which are typical functional components of cardiac muscle [54]. Importantly, there are matured sarcomeres (Sm) between two Z lines (ZL, or Z discs) with an average length of 1.7 ± 0.1 μm and width of 0.6 ± 0.1 μm (Fig. 5b) inside the myofibril. The abundant mitochondria (Mt) and SR support the contractile function of the sarcomeres (Fig. 5a–c) by providing energy and calcium, respectively [55]. There are also plenty of gap junctions (GJ) [56] and intercalated discs (iCD) located between the cell-cell membranes, which suggests a matured state of these ultrafine structures for signal transduction between CMs in the CSs (Fig. 5c). Moreover, there are CMs with multiple nuclei (Nu) per cell, which indicates the maturation of CMs (Fig. 5d). Collectively, the TEM data indicate critical ultrastructural evidence for the successful differentiation and maturation of CMs as early as day 12.5 post-cardiac differentiation.

We also conduct the calcium spike assay with the CSs on day 12.5 from the low RI group to examine their beating function, for which the fluo-4 staining is used to visualize the calcium transient in the CSs as shown in Movies 5-6. Furthermore, cardiac drugs isoproterenol (ISO) that speeds up beating and propranolol (PRO) that slows down beating are used to test the drug response of the CSs (Fig. 5e-f and Movies 7-8). Before the drug treatments, the CSs maintained a beating rate of 65 ± 13 beats per minute, similar to that of a healthy adult human heart. When treated with ISO, the beating rate is significantly increased to 93 ± 15 beats per minute. The beating rate is subsequently decreased to 26 ± 12 beats per minute after treating the CSs with PRO. Overall, this data shows that the CSs derived from eiPSCs with reduced RI concentration develop normal beating activities and may serve as an *in vitro* model for cardiac research and drug screening.

Supplementary video related to this article can be found at https://doi.org/10.1016/j.bioactmat.2021.07.013.

It is worth noting that the human eiPSC-derived homogeneous CSs are compatible with GelMA that has been widely used for 3D bioprinting. As shown in Fig. 5g and Movies 9-11, the CSs collected on day 5 post-cardiac differentiation (before the initiation of spontaneous beating) and homogeneously suspended/cultured in 7 % GelMA, fuse together within 2 days of culture in the GelMA. The fused cardiac spheroids start to beat together synchronously on day 7 post-cardiac

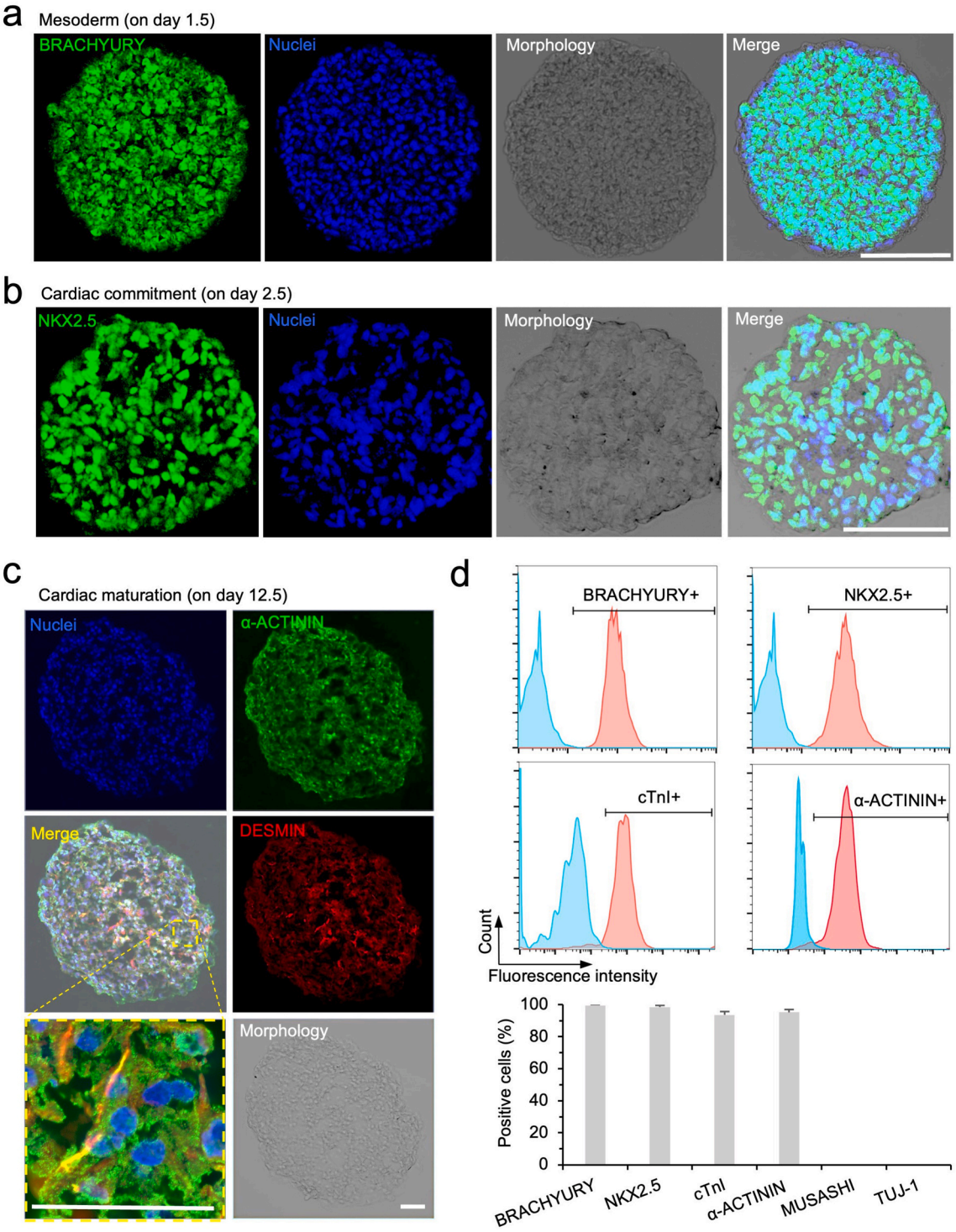

Fig. 4. Characterization of the stage-specific protein markers for cardiac differentiation of eiPSC spheroids from the 1 μM RI culture. (**a**) Immunostaining data showing the cells in the spheroids on day 1.5 are positive for the mesoderm specific gene marker BRACHYURY, indicating successful mesoderm induction. Scale bar: 100 μm. (**b**) Immunostaining data showing the cells in the spheroids on day 2.5 are positive for the early cardiac commitment specific protein marker NKX2.5, indicating successful induction of cardiac commitment to turn the eiPSC spheroids into CSs. Scale bar: 100 μm. (**c**) Immunostaining data showing cells in the spheroids on day 12.5 are positive for the cardiac-specific protein markers α-ACTININ for sarcomeres and DESMIN for intermediate filaments that integrate sarcolemma and Z disks. The CSs are filled with sarcomeres and intermediate filaments indicating high development of myofibrils, as shown in the zoom-in view of the merged image. Scale bars: 50 μm. (**d**) Flow cytometry analyses showing highly positive expression for the stage-specific protein markers including BRACHYURY (~100 %) on day 1.5; NKX2.5 (~100 %) on day 2.5; and cTnI (93.9 %), α-ACTININ (95 %) on day 12.5; while the expression of neural-specific protein markers MUSASHI and TUJ-1 on day 12.5 is negative.

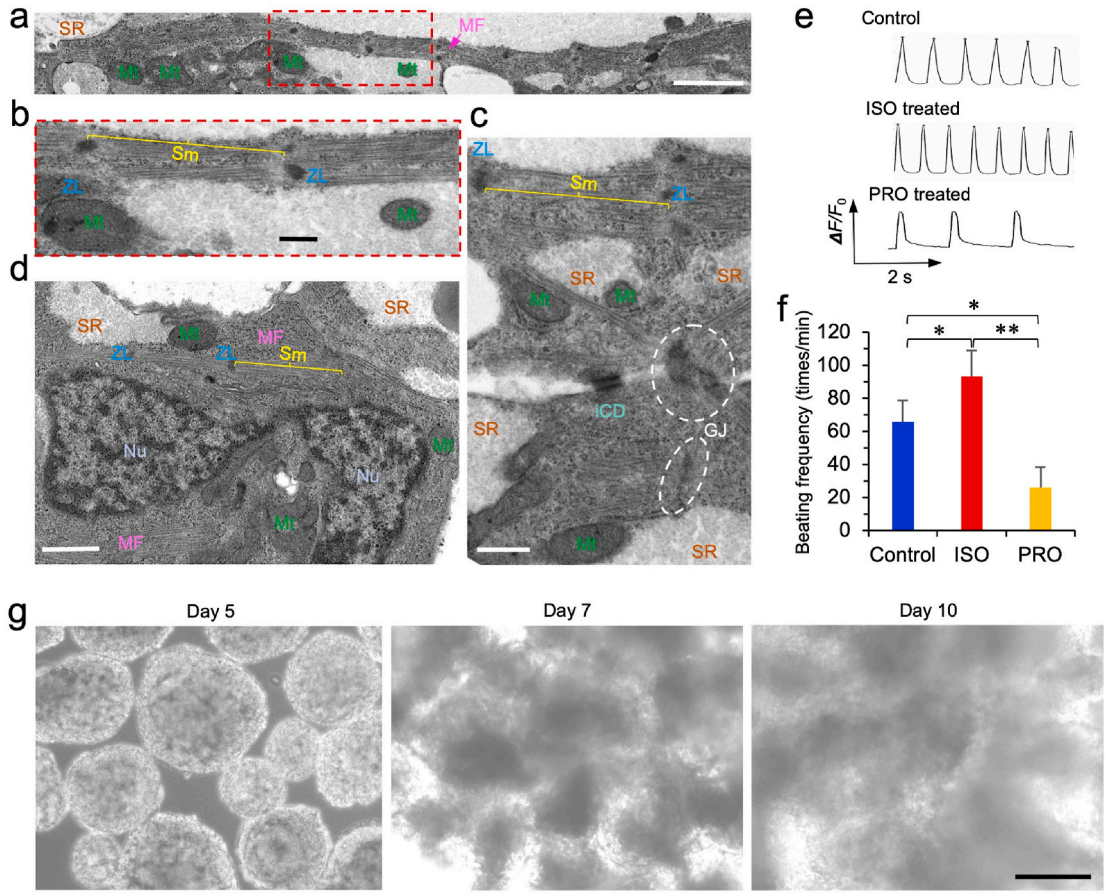

Fig. 5. Ultrastructural and functional analysis of the cardiac spheroids differentiated from eiPSC spheroids from the 1 μM RI culture. All CSs are collected on day 12.5. (**a**) A transmission electron microscopy (TEM) image showing a well-extended myofibril (MF) with a sarcoplasmic reticulum (SR), and multiple mitochondria (Mt) [55] located nearby in the CSs. Scale bar: 2 μm. (**b**) A zoom-in view of the dashed red box area in (**a**) showing well-organized sarcomere (Sm) with aligned Z lines (ZL) in the myofibril. Scale bar: 500 nm. (**c**) A TEM image showing abundant Mt, SR, intercalated disc (iCD), and gap junctions (GJ) [56] in the CSs. Scale bar: 250 nm. (**d**) A TEM image showing abundant Mt, SR, and two nuclei (Nu) in a CM in the CSs, indicating the formation of multinucleated CMs. Scale bar: 500 nm. (**e**) Representative calcium transients of CSs on day 12.5 before (control) and after treated with cardiac drugs isoproterenol (ISO, 1 μM) that increase the rate of heartbeat and propranolol (PRO, 1 μM) that decreases the rate of heartbeat, showing the responsiveness of the CSs to the cardiac drugs. F is the fluorescence intensity of calcium stain, F_0 is the fluorescence intensity of calcium stain at the resting state of the CSs, and $\Delta F = (F–F_0)$ is the change of the fluorescence intensity of calcium stain from the resting state. (**f**) Quantitative data on the beating frequency of CSs collected on day 12.5 before (control) and after treated the cardiac drugs ISO and PRO, showing ISO and PRO increase and decrease the beating frequency of the CSs, respectively. *, $p < 0.05$, and **, $p < 0.01$. (**g**) Morphology of the construct of the 7 % GelMA hydrogel suspended with cardiac spheroids (collected on day 5 post-initiation of cardiac differentiation) from the 1 μM RI group without culture and after cultured for 2 (on day 7) and 5 days (on day 10). The cardiac spheroids fuse together to beat synchronously after the 2–5 days of culture in the GelMA hydrogel (see Movies 9, 10, and 11 for days 5, 7, and 10, respectively). Scale bar: 200 μm.

differentiation, and they further merge into each other and beat synchronously and strongly as a whole with further culture in the GelMA to day 10. These data indicate the great potential of the CSs differentiated from the eiPSCs 3D-cultured with low RI for functional 3D cardiac tissue engineering and regenerative medicine applications.

Supplementary video related to this article can be found at https://doi.org/10.1016/j.bioactmat.2021.07.013.

2.5. High-quality 3D cardiac differentiation of IMR90-1 iPSCs cultured in 3D with low RI

Last but not the least, to confirm the much improved cardiac differentiation of iPSCs with low RI for their 3D culture before differentiation is not because of the human eiPSCs used, it is further tested with another commonly utilized human iPSC line (IMR90-1) [57]. As shown in Fig. 6a, the beating of the resultant IMR90-1 CSs is peaked at ~98% on day 7.5 with the OBT being synchronized within ~1 day for the 1 μM RI group. In contrast, only 11.5% of the IMR90-1 CSs beat on day 7.5 and the beating percentage increases to 34.1 % in a week, although it does not seem to change significantly after approximately day 10 for the 10 μM RI group. This is consistent with the flow cytometry data of the cells in the CSs collected on day 12.5, showing that 91 % and 32 % of the cells are positive for the cardiac-specific protein cTnT (that are crucial for beating) in the 1 and 10 μM RI groups, respectively (Fig. 6b–c). Furthermore, cells in the CSs that are positive for neural-specific maker MUSASHI are negligible in the 1 μM RI group, while ~20 % cells in the CSs from the 10 μM RI group are MUSASHI positive (Fig. 6b–c). The undesired neural differentiation in the 10 μM RI group is further confirmed by immunostaining data showing the existence of MUSASHI and TUJ-1-positive cells in the CSs collected on day 12.5, while the expression of both neural markers is negligible in the CSs from the 1 μM RI group (Fig. 6d). Moreover, the expression of the cardiac-specific protein cTnT is high with an evident expression of the gap junction protein CX-43 in the CSs of the 1 μM RI group, while the expression of cTnT and CX-43 is low and negligible, respectively, in the CSs of the 10 μM RI group (Fig. 6e). Again, these data from the IMR90-1 iPSCs confirm the observation that using a high RI in 3D culture to obtain iPSC spheroids causes heterogeneous lineage-commitment, which compromises the efficiency and quality of their subsequent cardiac differentiation.

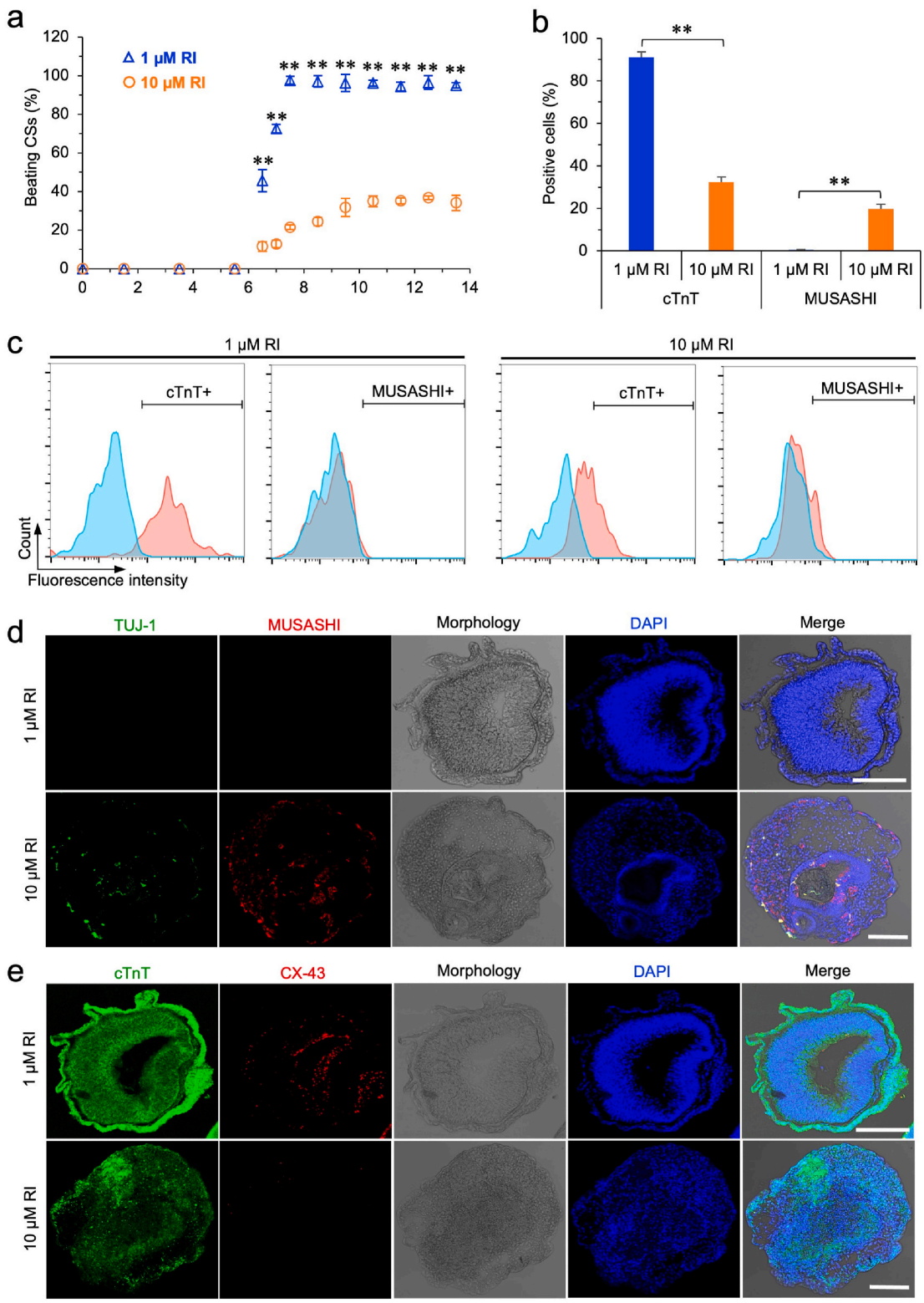

Fig. 6. Validation of the optimized protocol for cardiac differentiation using the IMR90-1 human iPSCs. (**a**) Quantitative data showing the percentage of beating IMR90-1 CSs over time during a period of 13.5 days post initiation of cardiac differentiation. Approximately 98 % of the IMR90-1 CSs in the 1 μM RI groups start to beat within 24 h, while only 34.1 % of the IMR90-1 CSs are observed to beat over 7 days (from day 6–6.5 to day 13.5) for the 10 μM RI group. (**b**) Quantitative data from flow cytometry analyses showing a significantly higher percentage of cTnT (cardiac-specific marker) positive cells and a significantly lower percentage of MUSASHI (neural-specific marker) cells in the CSs (collected on day 12.5) from the 1 μM RI group than the 10 μM RI group. Moreover, the expression of MUSASHI in the CSs of the 1 μM RI group is negligible while it is evident in the CSs of the 10 μM RI group. (**c**) Representative peaks of flow cytometry analyses showing a comparison of the expression of cTnT and MUSASHI in the CSs (collected on day 12.5) from the 1 and the 10 μM RI groups. (**d**) Immunostaining data showing cells positive for the neural gene markers (TUJ-1 and MUSASHI) are evident in the IMR90-1 CSs (collected on day 12.5) from the 10 μM RI group, while it is not observable for the 1 μM RI group. (**e**) Immunostaining data showing reduced expression of cTnT and CX-43 in the IMR90-1 CSs (collected on day 12.5) from the 10 μM RI group, while their expression is higher in the IMR90-1 CSs (collected on day 12.5) from the 1 μM RI group. Scale bars: 100 μm **, $p < 0.01$.

3. Discussion

Compared to human ESCs, human iPSCs have no ethical concerns and are more easily accepted by society because they are not from human embryos. Of note, human iPSC banks may be established for generating human leukocyte antigen (HLA)-matched cell transplantation for known HLA types of donors and recipients, and the human iPSCs have great potential for allogeneic cell therapy besides autologous cell therapy [58]. Furthermore, the human eiPSCs used in this study are virus-free [38], which further enhances the translational value of this work.

The iPSCs may not be the same as the ESCs in terms of both pluripotency and differentiation potential due to the iPSCs' epigenetic "memory" of their somatic tissues of origin [59,60]. This means the human iPSC may still possess some of the phenotypic properties of the more differentiated cells from which they are reprogrammed, leading to less potent potential of differentiation of human iPSCs than human ESCs [59,61]. Therefore, protocols of cardiac differentiation for human ESCs may not work well for human iPSCs and usually have an OBT ranging over ~7 days [31,62,63]. This is consistent with our observation that cardiac differentiation of the human eiPSCs and IMR90-1 iPSCs cultured in 3D with the commonly used RI concentration (10 μM) results in significantly heterogeneous cell populations and compromises the efficiency of cardiac differentiation, although the high concentration of RI has been used to culture human ESCs for cardiac differentiation (mostly under 2D) with high efficiency (the cTnT-positive cells may be up to 90 %) [26,35,36]. Moreover, the 3D culture has superiorities over the 2D culture for large-scale cell production and quality control [21]. Therefore, there is an urgent need to develop a stable system to upscale the generation of human iPSC-derived CMs for both basic and translational applications. However, the contemporary protocols for the derivation of human CSs in 3D are mainly human ESC-based, which have limitations regarding concerns of heterogeneous differentiation when applied on human iPSCs as aforementioned [60,64,65].

RI has been ubiquitously used to improve the survival/yield of human iPSCs and ESCs at a concentration of 10 μM, which is the optimal concentration for preventing apoptosis of the human PSCs under both 2D and 3D cultures [37,66,67]. Indeed, our data show that, with all other conditions being kept consistent, using 10 μM RI in the medium for culturing the eiPSCs in 3D significantly improves the cell yield (i.e., number of viable cells) by ~3 and 2 times, compared to 0 or 1 μM RI, respectively (Fig. S13). The use of 1 μM RI significantly increases the cell survival/yield compared to the 0 μM RI control (Fig. S13). Unfortunately, our extensive data of gene and protein expression show the RI at 10 μM induces uncontrolled spontaneous differentiation of the human eiPSCs into heterogeneous lineages including the ectoderm (e.g., neural and eye development), endoderm (e.g., lung and gut development), and non-cardiac mesoderm (e.g., urogenital and cartilage development) both before (i.e., on days −4 to 0, Fig. 1a) and after (i.e., after day 0, Fig. 1a) cardiac differentiation (Fig. 1c–f, 2, 3, S7-S12). The heterogeneous differentiation of human eiPSCs cultured with 10 μM RI before cardiac differentiation is also evidenced by the archenteron-like cavity of the eiPSC spheroid, similar to the epiblast and hypoblast cells in the early gastrula (Figs. S1a-b and S10b). Such heterogeneous differentiation into the ectoderm is further confirmed with the IMR90-1 iPSCs (Fig. 6d). Although RI promotes ectoderm differentiation from PSCs has been reported before [68,69], no prior work has reported not only its promotion of endoderm and non-cardiac mesoderm differentiation but also its adverse impact on cardiac differentiation. This uncontrolled spontaneous differentiation into heterogeneous lineages is shown to greatly compromise the efficiency and functional homogeneity (in terms of OBT) of guided cardiac differentiation of both the eiPSCs and IMR90-1 iPSCs cultured with the 10 μM RI in 3D (Figs. 1b and 6a). In stark contrast, the use of 1 μM RI results in more than 95 % beating CSs for cardiac differentiation of both the human eiPSCs and IMR90-1 iPSCs with the OBT being synchronized within 24 h (compared to >7 days for the 10 μM RI group), indicating a highly efficient and homogeneous (in terms of CM functional maturity judged by the much-shortened range of OBT) cardiac differentiation. This is attributed to the high pluripotency/quality of the human iPSCs cultured with 1 μM RI in the solid inner cell mass-like spheroids (Figs. 2f, 3, S1a-b, S7, S8, S10a, S11). It is worth noting that the size distribution (mostly 210–310 μm on day 0, Fig. S1c) of the eiPSC spheroids used in this study is similar to that of hPSC spheroids used for cardiac differentiation in the literature [70,71]. The size distribution should not have any significant impact on the cell response to RI concentration in this study. This is because the size distribution of the eiPSC spheroids is not significantly different between the 1 and 10 μM RI groups (Fig. S1c), and the radii of all the eiPSC spheroids are smaller than the diffusion limit (~200 μm) of nutrients/wastes (that are similar to or bigger than the RI in terms of molecular weight) in highly cellularized tissue or cell aggregates [72,73].

Lastly, the data shown in Fig. 5g and Movies 9-11 demonstrate the great potential of the CSs differentiated from the eiPSCs cultured with low RI in 3D for functional 3D cardiac tissue engineering, regenerative medicine, and personalized drug screening of cardiotoxicity. However, further specification of the CMs into ventricular and atrial ones is crucial for bioprinting a human heart *in vitro*. In addition, the xenogeneic Knockout serum replacement (KOSR) and fetal bovine serum (FBS) used in the media for cardiac differentiation and maintenance, respectively, may be replaced with materials of human origin to further improve the translational value of the human iPSC-derived CMs for treating cardiac diseases in the clinic.

In summary, culturing human eiPSCs with high RI (10 μM) improves the survival/yield of the iPSCs under 3D culture, but greatly compromises their capacity of cardiac differentiation. By reducing the RI to 1 μM for 3D culture of eiPSCs, the cell survival/yield is significantly improved compared no RI, and the heterogeneous gene and protein expression (i.e., neural, lung, urogenital, and ear-like cell types) is effectively suppressed compared to 10 μM RI. This enables highly efficient and homogeneous/synchronized cardiac differentiation of the human eiPSCs to obtain high-quality CMs with well-developed functional ultrastructures, which is further confirmed with the IMR90-1 human iPSCs. This highly efficient and homogeneous/synchronized 3D cardiac differentiation is particularly advantageous for large-scale production of human CMs with similar maturity, which may be used either directly or to engineer functional 3D cardiac constructs for both understanding and treating the deadly heart diseases.

4. Materials and methods

4.1. Cell culture

The human eiPSCs (DF19-9-11T.H, WiCell, Madison, WI, USA) and IMR90-1 human iPSCs (WiCell) were cultured in Matrigel (Corning, Corning, NY, USA)-coated 6-well plate in an iPSC maintenance medium made of DMEM/F12 (Gibco) supplemented with bFGF (120 ng/ml, R&D Systems), TGF-β (1 ng/ml, R&D Systems), γ-aminobutyric acid (100 μg/ml, Sigma-Aldrich), LiCl 30 (μg/ml, Sigma-Aldrich), L-glutamine (100 μg/ml, Gibco), MEM non-essential amino acid (NEAA) solution (0.5 %, Gibco), $NaHCO_3$ (500 μg/ml, Sigma-Aldrich), chemically defined lipid concentrate (1 %, Invitrogen), sodium selenite (50 ng/ml, Sigma-Aldrich), bovine serum albumin (20 mg/ml, Sigma-Aldrich), β-mercaptoethanol (4 μl per 500 ml medium, Sigma-Aldrich). The cells were passaged twice a week at a ratio between 1:4 and 1:5 with Versene (ThermoFisher) consisting of 0.48 nM ethylenediamineetraacetic acid (EDTA) in 1x (by default) phosphate buffered saline (PBS).

To obtain 3D iPSC spheroids, the iPSC colonies under 2D culture at ~80 % confluence were treated with Versene for 2 min, rinsed with PBS, and further detached from the substrate by gentle pipetting. The detached iPSCs were re-suspended in mTeSR1 with RI (Selleck Chemicals, Houston, TX, USA) at 0, 1, 5, or 10 μM. Afterward, the medium was supplemented with 0.35 % (v/v) methylcellulose (R&D Systems,

Minneapolis, MN, USA). The cell suspension (12 ml) containing ~4 × 10^6 cells was pushed through a cell strainer (R&D Systems) with 100 μm mesh size as previously reported [23,26]. Later, the suspension of iPSC clumps was transferred into a 10-cm petri dish (ThermoFisher) for culture in a humidified incubator at 37 °C and 5 % CO_2 for 2 days, during which the 2D iPSC clumps grew into 3D iPSC spheroids. Then, the medium was changed to mTeSR1 (supplemented with 0.35 % methylcellulose) with no RI, to further culture for 2 days before cardiac differentiation. To determine the number of cells per eiPSC spheroid, roughly equal numbers of the spheroids from either the 1 or 10 μM RI group were pooled together and trypsinized to dissociate the cells. The dissociated cells were then resuspended in 1.4 ml of the aforementioned iPSC maintenance medium and the cell number was counted using a hemacytometer. Three independent runs with 282, 260, and 256 spheroids for the 1 μM RI group and 273, 298, and 286 spheroids for the 10 μM RI group were conducted.

4.2. Teratoma assay

To test the pluripotency of the cells in the 3D iPSC spheroids *in vivo* with the teratoma assay, the eiPSC spheroids were directly injected subcutaneously (s.c.) into the dorsal rear flank of severe combined immunodeficient mice (NOD.CB17-scid, Charles River, Wilmington, MA, USA). A total of 2 × 10^6 cells in 300 μL of PBS was injected into each mouse (age: 5 weeks, and 5 mice per group). After 5 weeks, the mice were sacrificed, and the resulting teratoma were collected and fixed in 4 % paraformaldehyde (PFA, Thermofisher) for 3 days. Afterward, the samples were cut into small pieces of ~0.5 cm^3, embedded in paraffin, and sectioned into slices of 5 μm thick. The slices were stained with hematoxylin and eosin (H&E) and imaged with a Zeiss (Oberkochen, Germany) LSM 710 microscope. All animal studies were approved by the Institutional Animal Care and Use Committee (IACUC, #R-MAY-18-24) at the University of Maryland, College Park.

4.3. Cardiac differentiation in 3D

As schematically illustrated in Fig. 1a, the eiPSC spheroids obtained after 4 days of culture on day 0 were induced into mesoderm by up-regulation of the Wnt signaling pathway using 8 μM CHIR99021 (ThermoFisher) and 2 μM GSK inhibitor 6-bromoindirubin-3′-oxime (BIO) (ThermoFisher) in the mesoderm induction medium for 1 day. The mesoderm induction medium is a mixture of DMEM/F12 (ThermoFisher) and α-MEM (ThermoFisher) (v/v, 1:1), containing 2 % Knockout Serum Replacement (KOSR, Gibco, Gaithersburg, MD, USA), 1 mM L-glutamine (Invitrogen, Carlsbad, CA, USA), 1 % MEM non-essential amino acids (NEAA, ThermoFisher), and 0.1 mM β-mercaptoethanol (Sigma-Aldrich, St. Louis, MO, US). After 1 day, the spheroids were induced for cardiac commitment by down-regulating the Wnt signaling pathway using 10 μM KY02111 (ThermoFisher) and 10 μM XAV939 (ThermoFisher) in the cardiac maintenance medium for 6 days with the medium being changed every other day. The cardiac maintenance medium was a mixture of RPMI1640 (ThermoFisher) and α-MEM (ThermoFisher) (v/v, 1:1), containing 5 % fetal bovine serum (FBS, Gibco). Starting from day 8, the cardiac maintenance medium without KY02111 and XAV939 was used and it was changed every other day for cardiac maturation. Images and videos of the resultant CSs were taken using the Zeiss LSM 710 microscope before medium change.

4.4. Cryosectioning and immunostaining

The iPSC spheroids and the iPSC-derived CSs were fixed in 4 % PFA in PBS at 4 °C overnight. The fixed spheroids were incubated sequentially in 10 % and 15 % sucrose solutions in saline for 4 h, respectively. Afterward, the spheroids were put in a plastic box (Tissue-Tek Sakura, Lakewood Ranch, FL, USA) and embedded in OCT (Tissue-Tek Sakura) for cryosectioning. Slices of the spheroids of 10 μm thick were obtained by cutting the frozen sample on a Leica (Buffalo Grove, IL, USA) cryostat platform and then immediately attached onto the Leica Apex high adhesive glass slides.

For immunostaining, the slides were gently rinsed twice with PBS to remove the OCT and then incubated with 0.1 % Triton X-100 (Sigma-Aldrich, to permeabilize the cells) and 5 % normal goat serum (Invitrogen, Carlsbad, CA, USA, to block non-specific binding) in PBS for 1 h at room temperature (RT). Later, the samples were incubated with primary antibodies at 4 °C overnight. The dilution and product information of the primary antibodies were as follows: OCT-4 (1:500 dilution, Cell Signaling Technologies, Danvers, MA, USA), NANOG (1:500 dilution, Cell Signaling Technologies), SSEA-4 (1:500 dilution, Cell Signaling Technologies), cTnT (1:500 dilution, Cell Signaling Technologies), CONNEXIN-43 (CX-43, 1:400 dilution, Santa Cruz Biotechnology, Dallas, TX, USA), DESMIN (1:500 dilution, Santa Cruz Biotechnology), α-ACTININ (1:500 dilution, Santa Cruz Biotechnology), BRACHYURY (1:500 dilution, Santa Cruz Biotechnology), NKX2.5 (1:500 dilution, Santa Cruz Biotechnology), NESTIN (1:500 dilution, Sigma-Aldrich), MUSASHI (1:500 dilution, Sigma-Aldrich), and TUJ-1 (1:500 dilution, Sigma-Aldrich). Afterward, the samples were rinsed with PBS thrice and then incubated with the associated secondary antibodies (goat anti-rabbit IgG FITC and goat-*anti*-mouse IgG PE, 1:1000 dilution, Invitrogen) in PBS for 1.5 h at RT. Lastly, the samples were rinsed with 1 ml of PBS for 3 min and the nuclei were stained with 1 μg/ml DAPI (Sigma-Aldrich) solution for 5 min at RT. The samples were imaged with the Zeiss LSM 710 microscope.

4.5. Scanning electron microscopy

For scanning electron microscopy (SEM), the eiPSC spheroids collected on day −3 were fixed by 4 % PFA in PBS at 4 °C overnight. Then, the spheroids were incubated in 15 % sucrose solution in saline for 4 h. Afterward, the spheroids were suspended in 100 % ethanol and loaded on the SEM sample carrier and dried at RT overnight. The samples were then sputter-coated with gold at 15 mA for 2 min using the Ted Pella (Redding, CA, USA) Cressington-108 sputter coater. SEM images of the spheroids were obtained with a Hitachi (Tokyo, Japan) SU-70 FEG scanning electron microscope.

4.6. Flow cytometry

For flow cytometry, the eiPSC spheroids were collected on day 0 and the CSs were collected on days 1.5, 2.5, 12.5, or 15. The spheroids were dissociated to single cells by 0.25 % trypsin (Gibco) for 5 min at 37 °C and then fixed with 75 % ethanol at 4 °C overnight. The cells were permeabilized with 0.05 % Triton X-100 (Sigma-Aldrich) for 3 min and then rinsed with 1x PBS twice. The cell numbers were adjusted to 1 × 10^6 cells/tube in 700 μL of saline for each marker. These cells were incubated with primary antibodies including OCT-4 (1:500 dilution, Cell Signaling Technologies), NANOG (1:500 dilution, Cell Signaling Technologies), SSEA-4 (1:500 dilution, Cell Signaling Technologies), BRACHYURY (1:500 dilution, Santa Cruz Biotechnology), NKX2.5 (1:500 dilution, Santa Cruz Biotechnology), cTnT (1:500 dilution, Cell Signaling Technologies), cTnI (1:500 dilution, Cell Signaling Technologies), α-ACTININ (1:500 dilution, Santa Cruz Biotechnology), MUSASHI (1:500 dilution, Sigma-Aldrich), and TUJ-1 (1:500 dilution, Sigma-Aldrich) at 4 °C overnight. Subsequently, the samples were rinsed with PBS thrice before incubation with corresponding secondary antibodies: goat anti-mouse IgG FITC and goat anti-rabbit IgG PE, respectively (1:1000 dilution, Invitrogen) for 1 h at RT. The samples were then rinsed

with 1x PBS thrice before flow cytometry. The negative controls were the cells incubated with respective primary antibodies as aforementioned (no incubation with a secondary antibody).

4.7. RNA sequencing

For RNA sequencing (RNA-Seq), total RNA was extracted from the eiPSC clumps from 2D culture on day −4 (termed as 2D) and spheroids collected on day −2.5 after 1.5 days in the 3D culture (termed as UO and UT for 1 μM and 10 μM RI conditions, respectively), day 2.5 (termed as CO and CT), and day 13.5 (termed as MO and MT) by using the RNeasy kit (QIAGEN, Hilden, Germany). The DNase I from bovine pancreas (Sigma-Aldrich) was used to remove DNA in samples. The RNA concentration in the samples was measured with Nanodrop (ThermoFisher) and the integrity and quality of RNAs in the samples were studied with the Nano RNA Bioanalyzer (Agilent, Santa Clara, CA, USA). Samples with RNA integrity number greater than 9 were used for the preparation of the next-generation sequencing library using the NEB Ultra Directional RNA library preparation kit (New England Biolabs, Ipswich, MA, USA). Pair-end sequencing was performed by the Illumina HiSeq2500 platform (San Diego, CA, USA). RNA-seq sequencing data quality was verified by Novogene (Sacramento, CA, USA). Raw reads were mapped to the human reference genome version (hg38) and the gene expression level based on reads per kilobase of exon per million reads mapped for annotated genes was measured and normalized using the Cufflink program [39]. Samples were compared in different combinations as described previously (Table 1) and genes with an expression change of more than 1.5 in $|\log_2 \text{fold change}|$ were defined as differentially expressed genes (DEG). Different classes of genes were subjected to functional and pathway analysis with the Gene Ontology (GO) database. The final data was visualized with Gene Cluster 3.0, Java Treeview 3.0, and Microsoft Excel 2010 software.

4.8. Transmission electron microscopy

For transmission electron microscopy (TEM) studies, the CSs collected on day 12.5 were fixed with 2.5 % glutaraldehyde, 2 % PFA, and 0.1 M PIPES buffer at pH 7.4 for 2 h at 4 °C, rinsed with PBS, and subsequently incubated with 1 % osmium tetroxide for 2 h at 4 °C. All the reagents used for preparing the samples were purchased from Sigma-Aldrich. Afterward, the samples were dehydrated by a series of ethanol solutions (75 %, 85 %, 95 %, and 100 %) and acetone sequentially. Then, the samples were embedded in the resin EMbed 812 (Araldite, PA, USA) by following the manufacturer's instructions. Slices (70 nm-thick) of the embedded samples were cut with a UC6 ultramicrotome (Leica) and subsequently stained with 1 % (w/v) uranyl acetate for 10 min at RT. The slices were examined and imaged with an FEI Tecnai T12 transmission electron microscope (Philips, Amsterdam, Netherlands). The lengths of myofibrils and sarcomeres were measured with the NIH (Bethesda, MD, USA) ImageJ (v1.52a).

4.9. Calcium spike assay

To quantify the calcium spike, the CSs collected on day 12.5 either without or with drug treatment were incubated with 2 nM Fluo-4 probes (ThermoFisher) in cardiac maintenance medium for 30 min by following the manufacturer's instructions. Then, the medium was replaced with fresh cardiac maintenance medium for 20 min. Afterward, the CSs were transferred into a 1 cm diameter glass-bottom dish containing 500 μL of cardiac maintenance medium and incubated in the stage incubator of the Zeiss LSM 710 microscope at 37 °C and 5 % CO_2 for imaging and video recording. Cardiac drugs Isoproterenol (ISO) and propranolol (PRO) that increase and decrease the heart beating rate, respectively, were used to test the drug response of the CSs [13]. To do this, cardiac maintenance medium containing 10 μM ISO was incubated with the CSs for 10 min. After acquiring the calcium spike activity with the ISO treatment, the medium with ISO was removed and the CSs were rinsed with fresh cardiac maintenance medium for 3 min. Then, the CSs were incubated with cardiac maintenance medium containing 10 μM PRO for 10 min and the calcium spike activity was recorded. All the video-recording was done at 5 frames per second for 1 min using the Zeiss LSM 710 microscope and analyzed with the Zeiss Zen Blue software. Calcium spike activities were collected from three independent experiments to quantify the beating frequency/rate of the CSs. The data of the calcium spikes of the CSs were presented as $\Delta F/F_0$, where F represents fluorescence intensity, F_0 is the fluorescence intensity at the resting state of the CSs, and ΔF ($=F–F_0$) is the change of fluorescence intensity.

4.10. Culture of CSs in gelatin methacrylol hydrogel

To synthesize gelatin methacrylol (GelMA), type A porcine skin gelatin (300 bloom; Sigma-Aldrich) was dissolved at 10 % (w/v) into PBS (ThermoFisher) at 50 °C for 20 min. Methacrylic anhydride (MA, Sigma-Aldrich) was added dropwise into the gelatin solution under vigorous stirring for 1 h (0.6 g of MA per gram of gelatin). The mixture was diluted with PBS to stop the reaction and centrifuged at 2000g for 2 min. To remove excess acid, the supernatant containing dissolved GelMA was collected and dialyzed (10 kDa molecular weight cutoff, ThermoFisher) against water. The dialyzed GelMA was then frozen, lyophilized, and stored at −80 °C. To make the GelMA solution suspended with CSs, the lyophilized GelMA was dissolved at 7 % (w/v) in the cardiac maintenance medium at 50 °C for 20 min. Irgacure 2959 (0.1 % (w/v), BASF) was added into the GelMA solution at 50 °C and stirred for 15 min. The resultant GelMA solution was slowly cooled to 37 °C before mixing it with the CSs collected on day 5 post-cardiac differentiation (before beating). The GelMA solution suspended with CSs was transferred into a well of 12-well plate (ThermoFisher) at 4×10^6 cells in 0.5 ml of the GelMA solution. The GelMA solution was crosslinked into GelMA hydrogel by exposing it to ultraviolet light at 5 mW cm^{-2} for 1 min. Lastly, 1 ml of the cardiac maintenance medium was added into the well and the medium was changed every other day.

5. Statistical analysis

All quantitative data were collected from at least three independent experiments. The data were presented as mean ± standard deviation. Student's t-test (two-tails, unpaired, and assuming equal variance) was performed for comparisons between two groups. A p value less than 0.05 was considered to be statistically significant. The statistical methods for analyzing the RNA-Seq are given in the Results section where the data are discussed.

Author contributions

X.H. and B.J. conceived the project; X.H. supervised the study; X.H. and B.J. designed the experiments; B.J. conducted all experiments with assistance from W.Q., J.S., and S.V.B.; X.H., B.J., and C.H. analyzed data; B.J. and S.V.B. wrote the draft manuscript; X.H., J.S., J.F., S.S., and Z.L. edited the manuscript. All authors approved the manuscript.

Data availability

The data that support the findings of this study are available from the corresponding author upon reasonable request.

CRediT authorship contribution statement

Bin Jiang: Conceptualization, Methodology, Investigation, Writing, Formal analysis. **Wenquan Ou:** Methodology, Investigation. **James G. Shamul:** Methodology, Writing. **Hao Chen:** Methodology, Formal analysis. **Sarah Van Belleghem:** Methodology, Writing. **Samantha**

Stewart: Writing. **Zhenguo Liu:** Writing. **John P. Fisher:** Writing. **Xiaoming He:** Conceptualization, Methodology, Resources, Writing, Formal analysis, Supervision, Project administration.

Declaration of competing interest

The authors declare that they have no known competing financial interests or personal relationships that could have appeared to influence the work reported in this paper.

Acknowledgments

This work was partially supported by grants from the Maryland Stem Cell Research Fund (#2021-MSCRFD-5660), National Institutes of Health (NIH R01EB023632), and National Science Foundation (NSF CBET-1831019). We thank Dr. Kimberly M. Stroka for generously providing us the human eiPSCs.

Appendix A. Supplementary data

Supplemental Information: Figs. S1–S13, Table S1, and Movies 1-11 and their captions.

Supplementary data to this article can be found online at https://doi.org/10.1016/j.bioactmat.2021.07.013.

References

[1] CDC, Heart disease facts. https://www.cdc.gov/heartdisease/facts.htm, 2020. (Accessed 16 August 2020).
[2] E.J. Benjamin, P. Muntner, A. Alonso, M.S. Bittencourt, C.W. Callaway, A. P. Carson, A.M. Chamberlain, A.R. Chang, S. Cheng, S.R. Das, F.N. Delling, L. Djousse, M.S.V. Elkind, J.F. Ferguson, M. Fornage, L.C. Jordan, S.S. Khan, B. M. Kissela, K.L. Knutson, T.W. Kwan, D.T. Lackland, T.T. Lewis, J.H. Lichtman, C. T. Longenecker, M.S. Loop, P.L. Lutsey, S.S. Martin, K. Matsushita, A.E. Moran, M. E. Mussolino, M. O'Flaherty, A. Pandey, A.M. Perak, W.D. Rosamond, G.A. Roth, U. K.A. Sampson, G.M. Satou, E.B. Schroeder, S.H. Shah, N.L. Spartano, A. Stokes, D. L. Tirschwell, C.W. Tsao, M.P. Turakhia, L.B. VanWagner, J.T. Wilkins, S.S. Wong, S.S. Virani, E. American Heart Association Council on, C. Prevention Statistics, S. Stroke Statistics, Heart disease and stroke statistics-2019 update: a report from the American heart association, Circulation 139 (10) (2019) e56–e528.
[3] M.A. Laflamme, C.E. Murry, Heart regeneration, Nature 473 (7347) (2011) 326–335.
[4] M.L. Steinhauser, R.T. Lee, Regeneration of the heart, EMBO Mol. Med. 3 (12) (2011) 701–712.
[5] K. Huang, S. Hu, K. Cheng, A new era of cardiac cell therapy: opportunities and challenges, Advanced healthcare materials 8 (2) (2019), e1801011.
[6] Y. Jiang, X.L. Lian, Heart regeneration with human pluripotent stem cells: prospects and challenges, Bioact Mater 5 (1) (2020) 74–81.
[7] G. Zhang, Q.S. Hu, E.A. Braunlin, L.J. Suggs, J.Y. Zhang, Enhancing efficacy of stem cell transplantation to the heart with a PEGylated fibrin biomatrix, Tissue Eng. 14 (6) (2008) 1025–1036.
[8] S.K. Sanganalmath, R. Bolli, Cell therapy for heart failure: a comprehensive overview of experimental and clinical studies, current challenges, and future directions, Circ. Res. 113 (6) (2013) 810–834.
[9] H. Vidarsson, J. Hyllner, P. Sartipy, Differentiation of human embryonic stem cells to cardiomyocytes for in vitro and in vivo applications, Stem Cell Rev Rep 6 (1) (2010) 108–120.
[10] I. Minami, K. Yamada, T.G. Otsuji, T. Yamamoto, Y. Shen, S. Otsuka, S. Kadota, N. Morone, M. Barve, Y. Asai, T. Tenkova-Heuser, J.E. Heuser, M. Uesugi, K. Aiba, N. Nakatsuji, A small molecule that promotes cardiac differentiation of human pluripotent stem cells under defined, cytokine- and xeno-free conditions, Cell Rep. 2 (5) (2012) 1448–1460.
[11] K. Takahashi, S. Yamanaka, Induction of pluripotent stem cells from mouse embryonic and adult fibroblast cultures by defined factors, Cell 126 (4) (2006) 663–676.
[12] N. Sun, M. Yazawa, J.W. Liu, L. Han, V. Sanchez-Freire, S.J. Hu, D. Ricardo, M. Butte, E. Ashley, M. Longaker, R. Robbins, J. Wu, Patient-specific induced pluripotent stem cell as a model for familial dilated cardiomyopathy, Circulation 124 (21) (2011) 130ra47.
[13] H. Chen, B. Jiang, J.G. Shamul, X. He, Image entropy-based label-free functional characterization of human induced pluripotent stem cell-derived 3D cardiac spheroids, Biosens. Bioelectron. 179 (2021) 113055.
[14] K. Ronaldson-Bouchard, S.P. Ma, K. Yeager, T. Chen, L. Song, D. Sirabella, K. Morikawa, D. Teles, M. Yazawa, G. Vunjak-Novakovic, Advanced maturation of human cardiac tissue grown from pluripotent stem cells, Nature 556 (7700) (2018) 239–243.
[15] B.M. Ogle, N. Bursac, I. Domian, N.F. Huang, P. Menasche, C.E. Murry, B. Pruitt, M. Radisic, J.C. Wu, S.M. Wu, J. Zhang, W.H. Zimmermann, G. Vunjak-Novakovic, Distilling complexity to advance cardiac tissue engineering, Sci. Transl. Med. 8 (342) (2016) 342ps13.
[16] H. Lu, Y. Li, Y. Wang, Y. Liu, W. Wang, Z. Jia, P. Chen, K. Ma, C. Zhou, Wnt-promoted Isl1 expression through a novel TCF/LEF1 binding site and H3K9 acetylation in early stages of cardiomyocyte differentiation of P19CL6 cells, Mol. Cell. Biochem. 391 (1–2) (2014) 183–192.
[17] S.J. Kattman, A.D. Witty, M. Gagliardi, N.C. Dubois, M. Niapour, A. Hotta, J. Ellis, G. Keller, Stage-specific optimization of activin/nodal and BMP signaling promotes cardiac differentiation of mouse and human pluripotent stem cell lines, Cell Stem Cell 8 (2) (2011) 228–240.
[18] X. Lian, J. Zhang, S.M. Azarin, K. Zhu, L.B. Hazeltine, X. Bao, C. Hsiao, T.J. Kamp, S.P. Palecek, Directed cardiomyocyte differentiation from human pluripotent stem cells by modulating Wnt/beta-catenin signaling under fully defined conditions, Nat. Protoc. 8 (1) (2013) 162–175.
[19] A.M. Smits, P. van Vliet, C.H. Metz, T. Korfage, J.P.G. Sluijter, P.A. Doevendans, M. J. Goumans, Human cardiomyocyte progenitor cells differentiate into functional mature cardiomyocytes: an in vitro model for studying human cardiac physiology and pathophysiology, Nat. Protoc. 4 (2) (2009) 232–243.
[20] I.O. Sirbu, X. Zhao, G. Duester, Retinoic acid controls heart anteroposterior patterning by down-regulating Isl1 through the Fgf8 pathway, Dev. Dynam. 237 (6) (2008) 1627–1635.
[21] P.W. Burridge, G. Keller, J.D. Gold, J.C. Wu, Production of de novo cardiomyocytes: human pluripotent stem cell differentiation and direct reprogramming, Cell Stem Cell 10 (1) (2012) 16–28.
[22] H. Kempf, C. Kropp, R. Olmer, U. Martin, R. Zweigerdt, Cardiac differentiation of human pluripotent stem cells in scalable suspension culture, Nat. Protoc. 10 (9) (2015) 1345–1361.
[23] T.G. Otsuji, J. Bin, A. Yoshimura, M. Tomura, D. Tateyama, I. Minami, Y. Yoshikawa, K. Aiba, J.E. Heuser, T. Nishino, K. Hasegawa, N. Nakatsuji, A 3D sphere culture system containing functional polymers for large-scale human pluripotent stem cell production, Stem cell reports 2 (5) (2014) 734–745.
[24] P. Agarwal, S. Zhao, P. Bielecki, W. Rao, J.K. Choi, Y. Zhao, J. Yu, W. Zhang, X. He, One-step microfluidic generation of pre-hatching embryo-like core-shell microcapsules for miniaturized 3D culture of pluripotent stem cells, Lab Chip 13 (23) (2013) 4525–4533.
[25] S. Zhao, P. Agarwal, W. Rao, H. Huang, R. Zhang, Z. Liu, J. Yu, N. Weisleder, W. Zhang, X. He, Coaxial electrospray of liquid core-hydrogel shell microcapsules for encapsulation and miniaturized 3D culture of pluripotent stem cells, Integr Biol (Camb) 6 (9) (2014) 874–884.
[26] B. Jiang, Z. Xiang, Z. Ai, H. Wang, Y. Li, W. Ji, T. Li, Generation of cardiac spheres from primate pluripotent stem cells in a small molecule-based 3D system, Biomaterials 65 (2015) 103–114.
[27] M.N.T. Le, K. Hasegawa, Expansion culture of human pluripotent stem cells and production of cardiomyocytes, Bioengineering (Basel) 6 (2) (2019) 48.
[28] A.C. Fijnvandraat, A.C. van Ginneken, P.A. de Boer, J.M. Ruijter, V.M. Christoffels, A.F. Moorman, R.H. Lekanne Deprez, Cardiomyocytes derived from embryonic stem cells resemble cardiomyocytes of the embryonic heart tube, Cardiovasc. Res. 58 (2) (2003) 399–409.
[29] Y. Guo, W.T. Pu, Cardiomyocyte maturation: new phase in development, Circ. Res. 126 (8) (2020) 1086–1106.
[30] I. Batalov, A.W. Feinberg, Differentiation of cardiomyocytes from human pluripotent stem cells using monolayer culture, Biomark. Insights 10 (Suppl 1) (2015) 71–76.
[31] B. Jiang, L. Yan, J.G. Shamul, M. Hakun, X.M. He, Stem cell therapy of myocardial infarction: a promising opportunity in bioengineering, Advanced Therapeutics 3 (3) (2020) 1900182.
[32] G. Vunjak-Novakovic, N. Tandon, A. Godier, R. Maidhof, A. Marsano, T.P. Martens, M. Radisic, Challenges in cardiac tissue engineering, Tissue Eng. B Rev. 16 (2) (2010) 169–187.
[33] I.Y. Shadrin, B.W. Allen, Y. Qian, C.P. Jackman, A.L. Carlson, M.E. Juhas, N. Bursac, Cardiopatch platform enables maturation and scale-up of human pluripotent stem cell-derived engineered heart tissues, Nat. Commun. 8 (1) (2017) 1825.
[34] R. Zweigerdt, R. Olmer, H. Singh, A. Haverich, U. Martin, Scalable expansion of human pluripotent stem cells in suspension culture, Nat. Protoc. 6 (5) (2011) 689–700.
[35] T.C. McDevitt, J.C. Angello, M.l. Whitney, H. Reinecke, S.D. Hauschka, C.E. Murry, P.S. Stayton, In vitro generation of differentiated cardiac myofibers on micropatterned laminin surfaces, J. Biomed. Mater. Res. 60 (2002) 472–479, 0021-9304 (Print)).
[36] J. Sia, P. Yu, D. Srivastava, S. Li, Effect of biophysical cues on reprogramming to cardiomyocytes, Biomaterials 103 (1878–5905) (2016) 1–11 (Electronic)).
[37] M. Amit, I. Laevsky, Y. Miropolsky, K. Shariki, M. Peri, J. Itskovitz-Eldor, Dynamic suspension culture for scalable expansion of undifferentiated human pluripotent stem cells, Nat. Protoc. 6 (5) (2011) 572–579.
[38] J. Yu, K. Hu, K. Smuga-Otto, S. Tian, R. Stewart, Slukvin II, J.A. Thomson, Human induced pluripotent stem cells free of vector and transgene sequences, Science 324 (5928) (2009) 797–801.
[39] C. Trapnell, D.G. Hendrickson, M. Sauvageau, L. Goff, J.L. Rinn, L. Pachter, Differential analysis of gene regulation at transcript resolution with RNA-seq, Nat. Biotechnol. 31 (1) (2013) 46–53.
[40] S. Lee, C.H. Seo, B. Lim, J.O. Yang, J. Oh, M. Kim, S. Lee, B. Lee, C. Kang, S. Lee, Accurate quantification of transcriptome from RNA-Seq data by effective length normalization, Nucleic Acids Res. 39 (1362–4962) (2011) e9 (Electronic)).
[41] M.S. Salleh, G. Mazzoni, J.K. Hoglund, D.W. Olijhoek, P. Lund, P. Lovendahl, H. N. Kadarmideen, RNA-Seq transcriptomics and pathway analyses reveal potential

regulatory genes and molecular mechanisms in high- and low-residual feed intake in Nordic dairy cattle, BMC Genom. 18 (1) (2017) 258.
[42] M.A. Harris, J. Clark, A. Ireland, J. Lomax, M. Ashburner, R. Foulger, K. Eilbeck, S. Lewis, B. Marshall, C. Mungall, J. Richter, G.M. Rubin, J.A. Blake, C. Bult, M. Dolan, H. Drabkin, J.T. Eppig, D.P. Hill, L. Ni, M. Ringwald, R. Balakrishnan, J. M. Cherry, K.R. Christie, M.C. Costanzo, S.S. Dwight, S. Engel, D.G. Fisk, J. E. Hirschman, E.L. Hong, R.S. Nash, A. Sethuraman, C.L. Theesfeld, D. Botstein, K. Dolinski, B. Feierbach, T. Berardini, S. Mundodi, S.Y. Rhee, R. Apweiler, D. Barrell, E. Camon, E. Dimmer, V. Lee, R. Chisholm, P. Gaudet, W. Kibbe, R. Kishore, E.M. Schwarz, P. Sternberg, M. Gwinn, L. Hannick, J. Wortman, M. Berriman, V. Wood, N. de la Cruz, P. Tonellato, P. Jaiswal, T. Seigfried, R. White, C. Gene Ontology, The Gene Ontology (GO) database and informatics resource, Nucleic Acids Res. 32 (Database issue) (2004) D258–D261.
[43] L. Tirosh-Finkel, A. Zeisel, M. Brodt-Ivenshitz, A. Shamai, Z. Yao, R. Seger, E. Domany, E. Tzahor, BMP-mediated inhibition of FGF signaling promotes cardiomyocyte differentiation of anterior heart field progenitors, Development 137 (18) (2010) 2989–3000.
[44] R. Szabo, J.P. Hobson, K. Christoph, P. Kosa, K. List, T.H. Bugge, Regulation of cell surface protease matriptase by HAI2 is essential for placental development, neural tube closure and embryonic survival in mice, Development 136 (2009) 2653–2663, 0950-1991 (Print)).
[45] V. Maier, C. Jolicoeur, H. Rayburn, N. Takegahara, A. Kumanogoh, H. Kikutani, M. Tessier-Lavigne, W. Wurst, R.H. Friedel, Semaphorin 4C and 4G are ligands of Plexin-B2 required in cerebellar development, Mol. Cell. Neurosci. 46 (1095–9327) (2011) 419–431 (Electronic)).
[46] J. Kele, E.R. Andersson, J.C. Villaescusa, L. Cajanek, C.L. Parish, S. Bonilla, E. M. Toledo, V. Bryja, J.S. Rubin, A. Shimono, E. Arenas, SFRP1 and SFRP2 dose-dependently regulate midbrain dopamine neuron development in vivo and in embryonic stem cells, Stem Cell. 30 (1549–4918) (2012) 865–875 (Electronic)).
[47] C.S. Hong, J.P. Saint-Jeannet, The b-HLH transcription factor Hes3 participates in neural plate border formation by interfering with Wnt/β-catenin signaling, Dev. Biol. 442 (1095–564X) (2018) 162–172 (Electronic)).
[48] J. Muhr, K.M. Ackerman, Embryology, Gastrulation, StatPearls, Treasure Island (FL), 2021.
[49] N. Moris, A. Martinez Arias, B. Steventon, Experimental embryology of gastrulation: pluripotent stem cells as a new model system, Curr. Opin. Genet. Dev. 64 (2020) 78–83.
[50] C. Merkel, C. Karner, T. Carroll, Molecular regulation of kidney development: is the answer blowing in the Wnt? Pediatr. Nephrol. 22 (11) (2007) 1825–1838.
[51] R. Prunskaite-Hyyryläinen, I. Skovorodkin, Q. Xu, I. Miinalainen, J. Shan, S. Vainio, Wnt4 coordinates directional cell migration and extension of the Müllerian duct essential for ontogenesis of the female reproductive tract, Hum. Mol. Genet. 25 (6) (2016) 1059–1073.
[52] S. Kobayashi, T. T, I. M, I. S, K. H, Z. Yw, M. J, H. Taniguchi, Reconstruction of human elastic cartilage by a CD44+ CD90+ stem cell in the ear perichondrium, Proc. Natl. Acad. Sci. U. S. A 108 (1091–6490) (2011) 14479–14484 (Electronic)).
[53] T. N, K. Cb, T. S, A. W, M. L, I. Hj, K. W, Induction of CD44 cleavage in articular chondrocytes, Arthritis Rheum. 62 (5) (2010) 1338–1348.
[54] B. Paes, P.D. Moco, C.G. Pereira, G.S. Porto, E.M. de Sousa Russo, L.C.J. Reis, D. T. Covas, V. Picanco-Castro, Ten years of iPSC: clinical potential and advances in vitro hematopoietic differentiation, Cell Biol. Toxicol. 33 (3) (2017) 233–250.
[55] C. Lorenz, P. Lesimple, R. Bukowiecki, A. Zink, G. Inak, B. Mlody, M. Singh, M. Semtner, N. Mah, K. Aure, M. Leong, O. Zabiegalov, E.M. Lyras, V. Pfiffer, B. Fauler, J. Eichhorst, B. Wiesner, N. Huebner, J. Priller, T. Mielke, D. Meierhofer, Z. Izsvak, J.C. Meier, F. Bouillaud, J. Adjaye, M. Schuelke, E.E. Wanker, A. Lombes, A. Prigione, Human iPSC-derived neural progenitors are an effective drug discovery model for neurological mtDNA disorders, Cell Stem Cell 20 (5) (2017) 659–674 e9.
[56] T.W. Theunissen, B.E. Powell, H. Wang, M. Mitalipova, D.A. Faddah, J. Reddy, Z. P. Fan, D. Maetzel, K. Ganz, L. Shi, T. Lungjangwa, S. Imsoonthornruksa, Y. Stelzer, S. Rangarajan, A. D'Alessio, J. Zhang, Q. Gao, M.M. Dawlaty, R.A. Young, N. S. Gray, R. Jaenisch, Systematic identification of culture conditions for induction and maintenance of naive human pluripotency, Cell Stem Cell 15 (4) (2014) 471–487.
[57] J. Yu, M.A. Vodyanik, K. Smuga-Otto, J. Antosiewicz-Bourget, J.L. Frane, S. Tian, J. Nie, G.A. Jonsdottir, V. Ruotti, R. Stewart, I.I. Slukvin, J.A. Thomson, Induced pluripotent stem cell lines derived from human somatic cells, Science 318 (2007) 1095–9203, 1917-1920.
[58] C.J. Taylor, S. Peacock, A.N. Chaudhry, J.A. Bradley, E.M. Bolton, Generating an iPSC bank for HLA-matched tissue transplantation based on known donor and recipient HLA types, Cell Stem Cell 11 (2) (2012) 147–152.
[59] K. Kim, A. Doi, B. Wen, K. Ng, R. Zhao, P. Cahan, J. Kim, M.J. Aryee, H. Ji, L. I. Ehrlich, A. Yabuuchi, A. Takeuchi, K.C. Cunniff, H. Hongguang, S. McKinney-Freeman, O. Naveiras, T.J. Yoon, R.A. Irizarry, N. Jung, J. Seita, J. Hanna, P. Murakami, R. Jaenisch, R. Weissleder, S.H. Orkin, I.L. Weissman, A.P. Feinberg, G.Q. Daley, Epigenetic memory in induced pluripotent stem cells, Nature 467 (7313) (2010) 285–290.
[60] O. Bar-Nur, H.A. Russ, S. Efrat, N. Benvenisty, Epigenetic memory and preferential lineage-specific differentiation in induced pluripotent stem cells derived from human pancreatic islet beta cells, Cell Stem Cell 9 (1) (2011) 17–23.
[61] H. Noguchi, C. Miyagi-Shiohira, Y. Nakashima, Induced tissue-specific stem cells and epigenetic memory in induced pluripotent stem cells, Int. J. Mol. Sci. 19 (4) (2018) 930.
[62] H. Kilpinen, A. Goncalves, A. Leha, V. Afzal, K. Alasoo, S. Ashford, S. Bala, D. Bensaddek, F.P. Casale, O.J. Culley, P. Danecek, A. Faulconbridge, P. W. Harrison, A. Kathuria, D. McCarthy, S.A. McCarthy, R. Meleckyte, Y. Memari, N. Moens, F. Soares, A. Mann, I. Streeter, C.A. Agu, A. Alderton, R. Nelson, S. Harper, M. Patel, A. White, S.R. Patel, L. Clarke, R. Halai, C.M. Kirton, A. Kolb-Kokocinski, P. Beales, E. Birney, D. Danovi, A.I. Lamond, W.H. Ouwehand, L. Vallier, F.M. Watt, R. Durbin, O. Stegle, D.J. Gaffney, Common genetic variation drives molecular heterogeneity in human iPSCs, Nature 546 (7658) (2017) 370–375.
[63] C. DeBoever, H. Li, D. Jakubosky, P. Benaglio, J. Reyna, K.M. Olson, H. Huang, W. Biggs, E. Sandoval, M. D'Antonio, K. Jepsen, H. Matsui, A. Arias, B. Ren, N. Nariai, E.N. Smith, A. D'Antonio-Chronowska, E.K. Farley, K.A. Frazer, Large-scale profiling reveals the influence of genetic variation on gene expression in human induced pluripotent stem cells, Cell Stem Cell 20 (4) (2017) 533–546.
[64] F. Laco, T.L. Woo, Q. Zhong, R. Szmyd, S. Ting, F.J. Khan, C.L.L. Chai, S. Reuveny, A. Chen, S. Oh, Unraveling the inconsistencies of cardiac differentiation efficiency induced by the GSK3beta inhibitor CHIR99021 in human pluripotent stem cells, Stem Cell Reports 10 (6) (2018) 1851–1866.
[65] D. Nukaya, K. Minami, R. Hoshikawa, N. Yokoi, S. Seino, Preferential gene expression and epigenetic memory of induced pluripotent stem cells derived from mouse pancreas, Gene Cell. 20 (5) (2015) 367–381.
[66] M. Amit, J. Chebath, V. Margulets, I. Laevsky, Y. Miropolsky, K. Shariki, M. Peri, I. Blais, G. Slutsky, M. Revel, J. Itskovitz-Eldor, Suspension culture of undifferentiated human embryonic and induced pluripotent stem cells, Stem Cell Rev Rep 6 (2) (2010) 248–259.
[67] K. Watanabe, M. Ueno, D. Kamiya, A. Nishiyama, M. Matsumura, T. Wataya, J. B. Takahashi, S. Nishikawa, S. Nishikawa, K. Muguruma, Y. Sasai, A ROCK inhibitor permits survival of dissociated human embryonic stem cells, Nat. Biotechnol. 25 (6) (2007) 681–686.
[68] M. Maldonado, R.J. Luu, M.E. Ramos, J. Nam, ROCK inhibitor primes human induced pluripotent stem cells to selectively differentiate towards mesendodermal lineage via epithelial-mesenchymal transition-like modulation, Stem Cell Res. 17 (2) (2016) 222–227.
[69] Y. Kamishibahara, H. Kawaguchi, N. Shimizu, Rho kinase inhibitor Y-27632 promotes neuronal differentiation in mouse embryonic stem cells via phosphatidylinositol 3-kinase, Neurosci. Lett. 615 (2016) 44–49.
[70] P.W. Burridge, D. Anderson, H. Priddle, M.D. Barbadillo Munoz, S. Chamberlain, C. Allegrucci, L.E. Young, C. Denning, Improved human embryonic stem cell embryoid body homogeneity and cardiomyocyte differentiation from a novel V-96 plate aggregation system highlights interline variability, Stem Cell. 25 (4) (2007) 929–938.
[71] C.L. Mummery, J. Zhang, E.S. Ng, D.A. Elliott, A.G. Elefanty, T.J. Kamp, Differentiation of human embryonic stem cells and induced pluripotent stem cells to cardiomyocytes: a methods overview, Circ. Res. 111 (3) (2012) 344–358.
[72] P. Agarwal, H. Wang, M. Sun, J. Xu, S. Zhao, Z. Liu, K.J. Gooch, Y. Zhao, X. Lu, X. He, Microfluidics enabled bottom-up engineering of 3D vascularized tumor for drug discovery, ACS Nano 11 (7) (2017) 6691–6702.
[73] R.K. Jain, Normalization of tumor vasculature: an emerging concept in antiangiogenic therapy, Science 307 (5706) (2005) 58–62.